

Low energy phenomena of the lepton sector in an A_4 symmetry model with heavy inverse seesaw neutrinos

T. Phong Nguyen,^{1,*} T.T. Thuc,^{2,†} D.T. Si,^{3,‡} T. T. Hong,^{4,§} and L. T. Hue^{5,6,¶}

¹Department of Physics, Can Tho University,

3/2 Street, Ninh Kieu, Can Tho City 94000, Vietnam

²Department of Education and Training of Ca Mau, 70 Phan Dinh Phung, Vietnam

³Can Tho Department of Education and Training, Can Tho City 94000, Vietnam

⁴An Giang University, VNU - HCM, Ung Van Khiem Street,

Long Xuyen, An Giang 88000, Vietnam

⁵Subatomic Physics Research Group,

Science and Technology Advanced Institute,

Van Lang University, Ho Chi Minh City 70000, Vietnam

⁶Faculty of Technology, Van Lang University,

Ho Chi Minh City 70000, Vietnam

Abstract

An extension of the two Higgs doublet model including inverse seesaw neutrinos and neutral Higgs bosons was constructed based on the A_4 symmetry in order to explain the recent neutrino oscillation data. This model can distinguish two well-known normal and inverted order schemes of neutrino data once both the effective masses m_β in tritium beta decays and $\langle m \rangle$ in the neutrinoless double beta decay are observed. The lepton flavor violating decays of the charged leptons $e_b \rightarrow e_a \gamma$, $\mu \rightarrow 3e$, the Standard model-like Higgs boson decays $h \rightarrow e_b e_a$, and the μ -e conversions in some nuclei are generated from loop corrections. The experimental data of the branching ratio $\text{Br}(\mu \rightarrow e \gamma, 3e)$ predict that the upper bounds of $\text{Br}(\tau \rightarrow \mu \gamma, e \gamma)$ and $\text{Br}(h \rightarrow e_a e_b)$ are much smaller than the planned experimental sensitivities. In contrast, the μ -e conversions are the promising signals for experiments.

PACS numbers:

*Electronic address: thanhphong@ctu.edu.vn

†Electronic address: truongtrongthuck17@gmail.com

‡Electronic address: dangtrungsi@cantho.edu.vn

§Electronic address: tthong@agu.edu.vn

¶Electronic address: lethohue@vlu.edu.vn

I. INTRODUCTION

Observation of neutrino oscillation requires that models beyond the Standard Model (BSM) must be considered to explain both properties of the tiny active neutrino masses and the structure of the lepton mixing matrix U_{PMNS} named as the Pontecorvo-Maki-Nakagawa-Sakata (PMNS) matrix. The simple tri-bi maximal (TB) form of U_{PMNS} was introduced in Refs. [1–4], which can be explained theoretically as the consequence of discrete symmetries such as A_4 group [5–8]. The TB form implies exact zero value of a mixing angle θ_{13} defined in the standard form of U_{PMNS} [9] which is inconsistent with non-zero but small θ_{13} pointed out by experiments so that this form must be modified, see a recent review in Ref. [10]. Various modifications were carried out in order to looking for models as simple as possible [10–32]. Many of them are A_4 models generating active neutrino masses based on the well-known standard seesaw (SS) mechanism [20–23], some of them based on the inverse seesaw (ISS) [25].

In the A_4 models containing heavy neutrinos to generate active neutrinos through the SS or ISS mechanisms, the lepton flavor violating (LFV) couplings of neutrinos will give loop corrections to many LFV processes such as the decays of charged leptons (cLFV) $e_b \rightarrow e_a \gamma$, $\mu \rightarrow 3e$, decays of the Standard Model-like (SM-like) Higgs boson (LFVHD) $h \rightarrow e_a^+ e_b^-$, and the μ - e conversions in nuclei. For the standard SS models, these corrections to the LFVHD are very suppressed [33], therefore only the branching ratio (Br) of the decays $\mu \rightarrow e \gamma$ may reach experimental sensitivities. In contrast, using the so-called Casas-Ibarra parametrization [34] and the simple diagonal form of heavy neutrino mass matrix to determine the mixing parameters and neutrino masses, many ISS models predict large LFV corrections from heavy neutrinos to LFVHD [35–38]. Namely, $\text{Br}(h \rightarrow \tau \mu, \tau e)$ can reach the order of $\mathcal{O}(10^{-5})$ under the very small experimental constraint $\text{Br}(\mu \rightarrow e \gamma) < \mathcal{O}(10^{-13})$. Notice that the recent upper bounds of LFVHD at 95% confidence level are $\text{Br}(h \rightarrow \mu e) < 6.1 \times 10^{-5}$ (ATLAS), 3.5×10^{-4} (CMS), and $\text{Br}(h \rightarrow \tau e, \tau \mu) < \mathcal{O}(10^{-3})$ (ATLAS, CMS) [39–42]. The future sensitivities at e^+e^- colliders [43] and ATLAS at LHC [44, 45] for the $\text{Br}(h \rightarrow \mu e)$ and $\text{Br}(h \rightarrow \mu \tau, e \tau)$ are hoped to be order of $\mathcal{O}(10^{-5})$ and $\mathcal{O}(10^{-4})$, respectively. In general, these sensitivities are still larger than the upper bounds predicted by the models containing only loop contributions to the LFVHD.

The most strict constraints from experiments for cLFV decays are $\text{Br}(\mu \rightarrow e \gamma) <$

4.2×10^{-13} and $\text{Br}(\mu^+ \rightarrow e^+e^+e^-) < 10^{-12}$ [46], with the respective planned sensitivities will be 6×10^{-14} and $\mathcal{O}(10^{-16})$ [47]. These two constraints often result in much smaller values of $\text{Br}(\tau \rightarrow \mu\gamma, e\gamma)$ than the recent experimental upper bounds, or even the planned sensitivities of $\mathcal{O}(10^{-9})$. These cLFV decays and the μ -e conversions in nuclei were also investigated in the standard SS models [48, 49] and ISS model [50], including the minimal supersymmetric (MSSM) versions [51, 52]. Depending on the specific structures of the Higgs and lepton sectors of different discrete symmetric models, the allowed regions satisfying all cLFV experimental bounds will predict different possibility to observe the LFVHD in the future experiments.

Based on the SS models containing two $SU(2)_L$ Higgs doublets transforming as A_4 singlets [11, 26], in this work we will introduce a non-supersymmetric $A_4 \times Z_3 \times Z_{11}$ model with the ISS mechanism (A_4 ISS) to generate active neutrino masses and U_{PMNS} enough to explain the recent oscillation data and allow low mass scale of heavy neutrinos. In addition, the LFV signals will be discussed as other promoting channels to constrain the parameter space. Our work also pay attention to the LFVHD, which is often ignored in discrete symmetric models because the SM-like Higgs boson is difficult to realize in complicated Higgs potentials of both SUSY and non-SUSY versions. To keep the Yukawa term unchanged in the original SUSY versions, the discrete symmetries Z_3 and Z_{11} are introduced to exclude unwanted terms appearing in the non-SUSY version. The model also consists of additional $SU(2)_L$ neutral Higgs singlets (flavon) enough to generate the active neutrino mass matrix corresponding to U_{PMNS} close to the TB form in a special degenerate limit of the two independent parameters in the heavy neutrino mass matrix. Using a deviate parameter $\tilde{\epsilon}$ to relaxing this limit will result in the real form of U_{PMNS} . The observable parameters defined by the standard form of U_{PMNS} will be determined based on the recent work [10]. Using this in the numerical investigation, we collected allowed regions of the parameter space to study low energy observable quantities such as effective neutrino masses related with the neutrinoless double beta ($0\nu\beta\beta$) and Tritium beta decay, the cLFV decays $e_b \rightarrow e_a\gamma$, $\mu \rightarrow 3e$, and $h \rightarrow e_ae_b$. We note that the decay $h \rightarrow e_ae_b$ were rarely discussed in previously in discrete symmetric models, including the SUSY versions. The numerical results of the allowed regions will be compared with previous works as well as the current and future experimental constraints. In contrast with original SS models [11, 26], in this work all allowed values of the Dirac phase δ are considered and the parameter $\tilde{\epsilon}$ is solved exactly in this A_4 ISS model. Hence the allowed

regions of parameters will be determined more exhausted, leading different predictions for the low energy observable quantities. In addition, different from the ISS models with the Casas-Ibarra parameterisation [34], the masses and the particular form of the total lepton mixing matrix of all neutrinos originated from the $A_4 \times Z_3 \times Z_{11}$ symmetric breaking will lead to new predictions for the LFV signals.

The A_4 ISS contains two $SU(2)_L$ Higgs doublets and only flavons, therefore it inherits many properties of the well-known two Higgs doublet models (2HDM) type I and II, see a review in Ref. [53]. Based on many discussions on the 2HDMs, we will constrain many important parameters affecting strongly on the signals of LFV processes predicted by the A_4 ISS model. Namely, the most important parameters are the ratio of the two vacuum expectation values (vev) of the two neutral components in the Higgs doublets t_β , the charged Higgs mass, and the parameter s_δ defining the deviation of the SM-like Higgs boson couplings between the A_4 ISS and the SM. Based on the experimental results from LHC searches and precision electroweak test, the recent constraints on the parameter spaces of the 2HDM related with the A_4 ISS model were discussed in detailed in Refs. [54–56]. In the future project of energy collision of 100 TeV, promising signals of heavy higgs bosons with masses at $\mathcal{O}(10)$ TeV were mentioned [57]. In direct signal of heavy Higgs bosons predicted by the 2HDM may also appear in the future e^+e^- colliders [58], where large allowed t_β corresponds to the alignment limit $s_\delta \rightarrow 0$. The predictions on cLFV signals may depend strongly on t_β , leading to another channel to determine which $SU(2)_L$ Higgs doublet generates quark masses, i.e. the information to distinguish the type I and II of the 2HDM.

This work is organized as follows. In section II, we introduce the A_4 ISS mechanism, constructing the analytic formulas of active neutrino masses and mixing parameters as functions of free parameters. We also give out the allowed regions of parameter space satisfying the recent neutrino oscillation data. The predictions of the effective neutrino masses corresponding to the two decays, neutrinoless double beta and Tritium beta are also discussed. In section III, important properties of the SM-like Higgs and charged Higgs bosons are summarized. Analytic formulas and numerical results relating to the LFV processes are separated into two sections IV and V. Finally, the summary of our new results is given in section VI. There are four appendices presenting more details on the product rules of the A_4 symmetry, the full Higgs potential, the one-loop formulas contributing to the LFV decay amplitudes.

II. THE A_4 ISS MODEL

A. The particle content and lepton masses

The non-Abelian A_4 is a group of even permutations of 4 objects and has $4!/2 = 12$ elements. The model has three one-dimension ($\underline{1}$, $\underline{1}'$, $\underline{1}''$) and one three-dimensional ($\underline{3}$) irreducible representations. The important properties of this group and its representations needed for model construction were reviewed in the appendix A. The transformations for leptons and scalars under the total symmetry $SU(2)_L \times U(1)_Y \times A_4 \times Z_3 \times Z_{11} \times U(1)_L$ as well as their VEVs of the A_4 ISS model is shown in Table I. Here L is the normal lepton

TABLE I: List of fermion and scalar fields, where $\psi^a = (\nu_{aL}, e_{aL})^T$ ($a = 1, 2, 3$) and $\omega = e^{2i\pi/3}$, and $\omega_{11} = e^{2i\pi/11}$.

Lepton	$SU(2)_L$	$U(1)_Y$	A_4	Z_3	Z_{11}	L	
$\overline{\psi^l} = (\overline{\psi^1}, \overline{\psi^2}, \overline{\psi^3})$	2^*	1	$\underline{3}^*$	1	ω_{11}^{-5}	-1	
e_R	1	-2	$\underline{1}$	1	ω_{11}^{-2}	1	
μ_R	1	-2	$\underline{1}'$	1	ω_{11}^{-2}	1	
τ_R	1	-2	$\underline{1}''$	1	ω_{11}^{-2}	1	
N_R	1	0	$\underline{3}$	ω	ω_{11}^3	1	
X_R	1	0	$\underline{3}$	ω	ω_{11}	-1	
Scalar							VEV
h_u	2	-1	$\underline{1}$	ω^2	ω_{11}^2	0	$\langle h_u \rangle = v_u$
h_d	2	1	$\underline{1}$	1	1	0	$\langle h_d \rangle = v_d$
ϕ_S	1	0	$\underline{3}$	ω	ω_{11}^{-4}	0	$\langle \phi_S \rangle = (v_S, v_S, v_S)$
ϕ_T	1	0	$\underline{3}$	1	ω_{11}^{-4}	0	$\langle \phi_T \rangle = (v_T, 0, 0)$
ξ'	1	0	$\underline{1}'$	ω	ω_{11}^{-4}	0	$\langle \xi' \rangle = u'$
ξ''	1	0	$\underline{1}''$	ω	ω_{11}^{-4}	0	$\langle \xi'' \rangle = u''$

number, two Abelian discrete symmetries are added in order to get the minimal Lagrangian generating lepton masses and mixing parameters consistent with experiments. The two

$SU(2)_L$ Higgs doublets are expanded around their VEVs as

$$h_u = \begin{pmatrix} v_u + \frac{S_u + iA_u}{\sqrt{2}} \\ H_u^- \end{pmatrix}, \quad h_d = \begin{pmatrix} H_d^+ \\ v_d + \frac{S_d + iA_d}{\sqrt{2}} \end{pmatrix}, \quad (1)$$

where the electric charge operator is well-known as $Q = T^3 + Y/2$.

Considering the effective operators up to five dimension (dim.) needed to generate masses of lepton, the Yukawa Lagrangian respecting the total symmetry consists of two parts. In particular, the first part is renormalizable as follows

$$-\mathcal{L}^r = f\bar{\psi}_L^l N_R h_u + x'_A \xi' (\bar{N}_L^c X_R)'' + x''_A \xi'' (\bar{N}_L^c X_R)' + x_B (\phi_S \bar{N}_L^c X_R) + \text{H.c.} \quad (2)$$

While the second part consisting of all effective operators of five dim., including all terms breaking the lepton number L relevant with neutrino masses, is

$$-\mathcal{L}^{5d} = [y_e (\phi_T \bar{\psi}_L^l) e_R + y_\mu (\phi_T \bar{\psi}_L^l)'' \mu_R + y_\tau (\phi_T \bar{\psi}_L^l)' \tau_R] \frac{h_d}{\Lambda} + \frac{\lambda_X (\tilde{h}_u h_d^*)}{2\Lambda} (\bar{X}_L^c X_R) + \text{H.c.} \quad (3)$$

Here Λ is the cut-off scale of the model under consideration, $\tilde{h}_u = i\sigma_2 h_u^*$, the charge conjugation of the neutral leptons N_R and X_R are $N_L^c \equiv P_L N^c = (N_R)^c = C(N_R)^T$ and $X_L^c = (X_R)^c$, respectively. After spontaneous symmetry breaking, the charged lepton mass matrix comes out diagonal with $m_e = \frac{y_e v_T v_d}{\Lambda}$, $m_\mu = \frac{y_\mu v_T v_d}{\Lambda}$, and $m_\tau = \frac{y_\tau v_T v_d}{\Lambda}$. Correspondingly, the Higgs doublet h_d plays a similar role to the SM Higgs doublet in generating charged lepton masses. Only the last term in Eq. (3) breaks the lepton number L with two units, giving neutrino mass term $\mu'_X \equiv (\lambda_X v_u v_d / \Lambda)$, which can be small so that the ISS mechanism can work. The non-renormalizable terms generating charged lepton masses can be seen as the tree level mass originated the exchange of the heavy vector-like leptons transforming as $E_{L,R} = (E_1, E_2, E_3)_{L,R}^T \sim (1, -2)_{(3,1,1,1)}$ with the total symmetry $(SU(2)_L, U(1)_Y)_{(A_4, Z_3, Z_{11}, L)}$.

The renormalizable Lagrangian relating with $E_{L,R}$ that respect the total symmetry is

$$-\mathcal{L}_E^Y = y_\psi^E (\bar{\psi}_L^l E_R) h_d + y_e^E (\bar{E}_L \phi_T) e_R + y_\mu^E (\bar{E}_L \phi_T)'' \mu_R + y_\tau^E (\bar{E}_L \phi_T)' \tau_R \\ + \Lambda \bar{E}_L E_R + \text{h.c.}, \quad (4)$$

where we assume that $\Lambda \gg v_S, v_T, u, u''$ so that all of the above Higgs bosons do not contribute significantly to very heavy vector-like lepton masses $E_{1,2,3}$. Therefore, $m_{Ea} \equiv \Lambda$ for all $a = 1, 2, 3$. The non-renormalizable terms are reduced from the diagrams given in Fig.1.

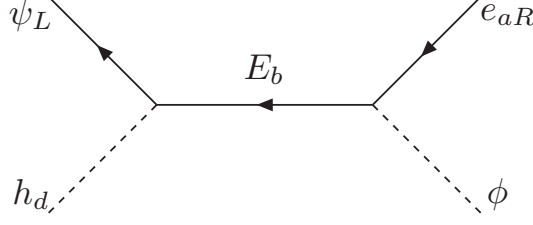


FIG. 1: Tree level diagrams generating effective terms given in Lagrangian (3).

For example in the regions where the vector-like lepton momenta are much smaller than their masses we the effective term $i\frac{y_e}{\Lambda}(\phi_T\bar{\psi}_L^l)e_R h_d \sim (iy_\psi^E)\bar{\psi}_L^l h_d \times \frac{i}{\Lambda} \times (iy_e^E)\phi_T e_R$.

The Lagrangian for neutrino mass is

$$-\mathcal{L}^\nu = \frac{1}{2} \begin{pmatrix} \bar{\nu}_L & \bar{N}_L^c & \bar{X}_L^c \end{pmatrix} \mathcal{M}^{\nu\dagger} \begin{pmatrix} (\nu_L)^c \\ N_R \\ X_R \end{pmatrix} + \text{h.c.}, \quad \mathcal{M}^\nu \equiv \begin{pmatrix} 0 & m_D^T & 0 \\ m_D & 0 & M_R^T \\ 0 & M_R & \mu_X \end{pmatrix}, \quad (5)$$

where m_D , M_R , and μ_X are 3×3 Dirac and Majorana neutrino mass matrices have the following forms

$$m_D = v_u f \times I_3 \equiv v_u Y_\nu, \quad (6)$$

$$M_R = M_0 \begin{pmatrix} 1 & \tilde{\kappa} - \frac{1}{2} & \tilde{\rho} - \frac{1}{2} \\ \tilde{\kappa} - \frac{1}{2} & \tilde{\rho} + 1 & -\frac{1}{2} \\ \tilde{\rho} - \frac{1}{2} & -\frac{1}{2} & \tilde{\kappa} + 1 \end{pmatrix} \equiv M_0 M_R^r, \quad \mu_X = \mu_X^{*'} \begin{pmatrix} 1 & 0 & 0 \\ 0 & 0 & 1 \\ 0 & 1 & 0 \end{pmatrix}, \quad (7)$$

and

$$M_0 \equiv \frac{2x_B^* v_S}{3}, \quad \tilde{\kappa} \equiv \frac{x_A^{*'} u''}{M_0} = \kappa e^{i\phi_1}, \quad \tilde{\rho} = \frac{x_A^{*'} u'}{M_0} \equiv \tilde{\kappa}(1 + \tilde{\epsilon}). \quad (8)$$

The tilde notation in \tilde{x} implies a complex parameter, and $x \equiv |\tilde{x}| > 0$. Without loss of generality, the real and positive M_0 is assumed in Eq. (8) and $0 \leq \phi_1 < 2\pi$. The effective neutrino mass matrix m_ν is then obtained by the ISS relations [59], which is a specific of the general SS framework [60, 61]:

$$m_\nu = m_D^T M_R^{-1} \mu_X (M_R^T)^{-1} m_D, \quad (9)$$

where

$$m_\nu \equiv U_{3\nu}^* \hat{m}_\nu U_{3\nu}^\dagger, \quad \hat{m}_\nu \equiv \text{diag}(m_{n_1}, m_{n_2}, m_{n_3}) \quad (10)$$

relating with the mixing matrix $U_{3\nu}$ and the masses m_{n_a} ($a = 1, 2, 3$) of the three active neutrinos, leading to the following form of the U_{PMNS} ,

$$U_{\text{PMNS}} = U_{L,e}^\dagger U_{3\nu}, \quad (11)$$

where $U_{L,e}$ is defined by the relation $U_{L,e}^\dagger m_D U_{R,e} = \text{diag}(m_e, m_\mu, m_\tau)$. The standard form of the U_{PMNS} is the unitary matrix defined as follows [9]

$$\begin{aligned} U_{\text{PMNS}}^{\text{PDG}} &= \begin{pmatrix} 1 & 0 & 0 \\ 0 & c_{23} & s_{23} \\ 0 & -s_{23} & c_{23} \end{pmatrix} \begin{pmatrix} c_{13} & 0 & s_{13}e^{-i\delta} \\ 0 & 1 & 0 \\ -s_{13}e^{i\delta} & 0 & c_{13} \end{pmatrix} \begin{pmatrix} c_{12} & s_{12} & 0 \\ -s_{12} & c_{12} & 0 \\ 0 & 0 & 1 \end{pmatrix} \text{diag} \left(1, e^{i\frac{\alpha_{21}}{2}}, e^{i\frac{\alpha_{31}}{2}} \right) \\ &= U_{\text{PMNS}}^0 \text{diag} \left(1, e^{i\frac{\alpha_{21}}{2}}, e^{i\frac{\alpha_{31}}{2}} \right), \end{aligned} \quad (12)$$

where $s_{ij} \equiv \sin \theta_{ij}$, $c_{ij} \equiv \cos \theta_{ij}$, $i, j = 1, 2, 3$ ($i < j$), $0 < \theta_{ij} < 180$ [Deg.] and $0 < \delta \leq 720$ [Deg.]. In this work, $U_{L,e} = U_{R,e} = I_3$, hence

$$U_{\text{PMNS}} = U_{3\nu} = \text{diag} (e^{i\psi_1}, e^{i\psi_2}, e^{i\psi_3}) U_{\text{PMNS}}^{\text{PDG}}, \quad (13)$$

where the phases $\psi_{1,2,3}$ are absorbed into the charged lepton states. The standard form $U_{\text{PMNS}}^{\text{PDG}}$ provides the experimental quantities s_{ij} and δ , α_{21} and α_{31} .

Let us remind that the TB framework of the lepton mixing matrix was predicted in an A_4 model with the standard SS mechanism. It also happens in this model in the degenerate condition that $\tilde{\rho} = \tilde{\kappa}$, corresponding to $\tilde{\epsilon} = 0$. As a result, the neutrino mixing matrix $U_{3\nu}$ given by Eq. (9) have the TB form:

$$U_{\text{TB}} = \begin{pmatrix} \sqrt{\frac{2}{3}} & \frac{1}{\sqrt{3}} & 0 \\ -\frac{1}{\sqrt{6}} & \frac{1}{\sqrt{3}} & -\frac{1}{\sqrt{2}} \\ -\frac{1}{\sqrt{6}} & \frac{1}{\sqrt{3}} & \frac{1}{\sqrt{2}} \end{pmatrix}, \quad (14)$$

corresponding to $s_{13} = 0$. This is in contrast with the experimental data of neutrino, which is divided into two cases of normal (NO) and inverted (IO) schemes. The best-fit and 3σ values for the NO are [9]

$$\begin{aligned} s_{12}^2 &= 0.31, \quad 0.275 \leq s_{12}^2 \leq 0.350; \\ s_{23}^2 &= 0.558, \quad 0.427 \leq s_{23}^2 \leq 0.609; \\ s_{13}^2 &= 0.02241, \quad 0.02046 \leq s_{13}^2 \leq 0.02440; \end{aligned}$$

$$\begin{aligned}
\delta &= 222 \text{ [Deg]}, 141 \text{ [Deg]} \leq \delta \leq 370 \text{ [Deg]}; \\
\Delta m_{21}^2 &= 7.39 \times 10^{-5} [\text{eV}^2], \quad 6.79 \times 10^{-5} [\text{eV}^2] \leq \Delta m_{21}^2 \leq 8.01 \times 10^{-5} [\text{eV}^2]; \\
\Delta m_{32}^2 &= 2.449 \times 10^{-3} [\text{eV}^2], \quad 2.358 \times 10^{-3} [\text{eV}^2] \leq \Delta m_{32}^2 \leq 2.544 \times 10^{-3} [\text{eV}^2]. \quad (15)
\end{aligned}$$

For the IO case, the values of s_{12} and Δm_{21}^2 are the same and

$$\begin{aligned}
s_{23}^2 &= 0.563, \quad 0.430 \leq s_{23}^2 \leq 0.612; \\
s_{13}^2 &= 0.02261, \quad 0.02066 \leq s_{13}^2 \leq 0.02461; \\
\delta &= 285 \text{ [Deg]}, 205 \text{ [Deg]} \leq \delta \leq 354 \text{ [Deg]}; \\
\Delta m_{32}^2 &= -2.509 \times 10^{-3} [\text{eV}^2], \quad -2.603 \times 10^{-3} [\text{eV}^2] \leq \Delta m_{32}^2 \leq -2.416 \times 10^{-3} [\text{eV}^2]. \quad (16)
\end{aligned}$$

We consider the real case, where all θ_{ij} is in the 3σ ranges of the experimental data. We assume a solution that the deviation from the TB data arises from only the condition that $\tilde{\rho} \neq \tilde{\kappa}$ in the matrix M_R given in Eq. (7), equivalently $\tilde{\epsilon} \neq 0$. Then, the mixing matrix $U_{3\nu}$ in Eq. (10) is calculated by writing it as

$$U_{3\nu} \equiv U_{\text{TB}} U_1 U_P, \quad U_P = \text{diag}(e^{-\frac{i\varphi_1}{2}}, e^{-\frac{i\varphi_2}{2}}, e^{-\frac{i\varphi_3}{2}}) \quad (17)$$

which can be identified with the well-known form given in Eq. (12). We then have,

$$\begin{aligned}
\hat{m}_\nu &= U_{3\nu}^T m_\nu U_{3\nu} = U_1^T m'_\nu U_1 = \text{diag}(m_{n_1}, m_{n_2}, m_{n_3}), \quad (18) \\
(U_{\text{TB}} U_1)^T m_\nu (U_{\text{TB}} U_1) &= \text{diag}(m_{n_1} e^{i\varphi_1}, m_{n_2} e^{i\varphi_2}, m_{n_3} e^{i\varphi_3}), \\
m'_\nu &\equiv U_{\text{TB}}^T m_\nu U_{\text{TB}}, \\
m'_\nu &= m_0 e^{-2i\phi_1} \begin{pmatrix} \frac{16(2\tilde{\epsilon}^2 - 2(3\tilde{\kappa}^{-1} + 2)\tilde{\epsilon} - (3\tilde{\kappa}^{-1} + 2)^2)}{\kappa^2(4\tilde{\epsilon}^2 + 4\tilde{\epsilon} - 9\tilde{\kappa}^{-2} + 4)^2} & 0 & \frac{32\sqrt{3}\tilde{\epsilon}(\tilde{\epsilon} + 2)}{\kappa^2(4\tilde{\epsilon}^2 + 4\tilde{\epsilon} - 9\tilde{\kappa}^{-2} + 4)^2} \\ 0 & -\frac{4}{\kappa^2(\tilde{\epsilon} + 2)^2} & 0 \\ \frac{32\sqrt{3}\tilde{\epsilon}(\tilde{\epsilon} + 2)}{\kappa^2(4\tilde{\epsilon}^2 + 4\tilde{\epsilon} - 9\tilde{\kappa}^{-2} + 4)^2} & 0 & -\frac{16(2\tilde{\epsilon}^2 + (6\tilde{\kappa}^{-1} - 4)\tilde{\epsilon} - (2 - 3\tilde{\kappa}^{-1})^2)}{\kappa^2(4\tilde{\epsilon}^2 + 4\tilde{\epsilon} - 9\tilde{\kappa}^{-2} + 4)^2} \end{pmatrix}, \quad (19)
\end{aligned}$$

where U_{TB} is given in Eq. (14) and

$$m_0 = \frac{f^2 \mu_X \nu_u^2}{4M_0^2} > 0. \quad (20)$$

The form of m'_ν results in the form of U_1 as follows:

$$U_1 = \begin{pmatrix} c_\theta & 0 & s_\theta e^{-i\phi_0} \\ 0 & 1 & 0 \\ -s_\theta e^{i\phi_0} & 0 & c_\theta \end{pmatrix}, \quad U_{\text{TB}} U_1 = \begin{pmatrix} \sqrt{\frac{2}{3}} c_\theta & \frac{1}{\sqrt{3}} & \sqrt{\frac{2}{3}} s_\theta e^{-i\phi_0} \\ \frac{s_\theta e^{i\phi_0}}{\sqrt{2}} - \frac{c_\theta}{\sqrt{6}} & \frac{1}{\sqrt{3}} & -\frac{c_\theta}{\sqrt{2}} - \frac{s_\theta e^{-i\phi_0}}{\sqrt{6}} \\ -\frac{c_\theta}{\sqrt{6}} - \frac{s_\theta e^{i\phi_0}}{\sqrt{2}} & \frac{1}{\sqrt{3}} & \frac{c_\theta}{\sqrt{2}} - \frac{s_\theta e^{-i\phi_0}}{\sqrt{6}} \end{pmatrix}. \quad (21)$$

where $c_\theta \equiv \cos \theta$, $s_\theta \equiv \sin \theta$, and ϕ_0 are real. The matrix U_1 is found by diagonalizing the matrix $m'_\nu m'^\dagger_\nu$, leading to the total the neutrino mixing matrix given in Eq. (21). It can be identified with the standard form given in Eq. (12) by the following relation [10, 62]

$$s_\theta^2 = \frac{3s_{13}^2}{2}, \quad s_{12}^2 = \frac{1}{3c_{13}^2}, \quad \cos \phi_0 = -\frac{(1 - s_{13}^2) \cos 2\theta_{23}}{s_{13} \sqrt{2 - 3s_{13}^2}}, \quad \cos \delta = \frac{\cos 2\theta_{13} \cos 2\theta_{23}}{s_{13} \sqrt{2 - 3s_{13}^2} \sin 2\theta_{23}}. \quad (22)$$

They were found by the requirement that $|(U_{\text{PMNS}}^0)_{ij}| = |(U_{\text{TB}}U_1)_{ij}|$ for all $i, j = 1, 2, 3$. These equations show that apart from θ, ϕ_0 , other parameters s_{12} and the Dirac phase can be written in terms of s_{13} and s_{23} . The formulas of $\cos \phi_0$ and $\cos \theta$ in (22) result in the following well-known relations [10]: $\sin \phi_0 = -\sin 2\theta_{23} \sin \delta$, and

$$\tan \phi_0 = (1 - \tan^2 \theta_{13}) \tan \delta. \quad (23)$$

Therefore, using $\tan^2 \phi_0 + 1 = 1/\cos^2 \phi_0$ and $\cos \phi_0/\cos \delta < 0$ to formulate $\cos \phi_0$ as follows

$$\cos \phi_0 = -\frac{\cos \delta}{\sqrt{1 + \sin^2 \delta \tan^2 \theta_{13} (\tan^2 \theta_{13} - 2)}}. \quad (24)$$

Based on Eq. (22), s_{23}^2 is written in term of the following function of δ and s_{13} ,

$$s_{23}^2 = \frac{1}{2} - \frac{\cos \delta s_{13} \sqrt{2 - 3s_{13}^2}}{2\sqrt{(3\sin^2 \delta + 1) s_{13}^4 - 2(\sin^2 \delta + 1) s_{13}^2 + 1}}. \quad (25)$$

From now on, s_{23} and ϕ_0 are investigated as the above functions of s_{13} and δ . The requirements $|\cos \phi_0|, |\sin \phi_0| \leq 1$ always satisfy under the recent 3σ data allowing only very small s_{13}^2 . In contrast, 3σ allowed range of s_{23}^2 gives an upper bound on δ , more strict than that from the 3σ experimental data as given in Fig. 2. The new upper bound of δ for both NO and IO schemes is

$$\delta < 5.5 \times 180/\pi \simeq 315 \text{ [Deg.]}. \quad (26)$$

Apart from relations in Eq. (22), the matrix $U_{\text{TB}}U_1$ casts into the well-known standard form:

$$U_{\text{TB}}U_1 = \text{diag}(e^{i\psi_1}, e^{i\psi_2}, e^{i\psi_3}) U_{\text{PMNS}}^0 \text{diag}(1, e^{i\gamma_2}, e^{i\gamma_3}), \quad (27)$$

where the unphysical phases ψ_i are absorbed into the charged lepton states. In contrast, the two phases $\gamma_{2,3}$ will contribute to the Majorana phases α_{ij} . By identifying $\text{Arg}[U_{\text{PMNS}}^0]_{ij} \equiv \delta_{ij} = \text{Arg}[\text{diag}(e^{-i\psi_1}, e^{-i\psi_2}, e^{-i\psi_3}) U_{\text{TB}}U_1 \text{diag}(1, e^{-i\gamma_2}, e^{-i\gamma_3})]_{ij}$, ψ_i and $\gamma_{2,3}$ are found as follows: $\psi_1 = 0 = \gamma_2 = \delta - \phi_0 - \gamma_3$, $\psi_2 = -\delta_{21} + \phi_{21} = \delta_{22} = -\gamma_3 + \phi_{23}$, and $\psi_3 = -\delta_{31} + \phi_{31} = \delta_{32} = -\gamma_3 + \phi_{33}$, where $\phi_{ij} \equiv \text{Arg}[U_{\text{TB}}U_1]_{ij}$. These equations are obtained

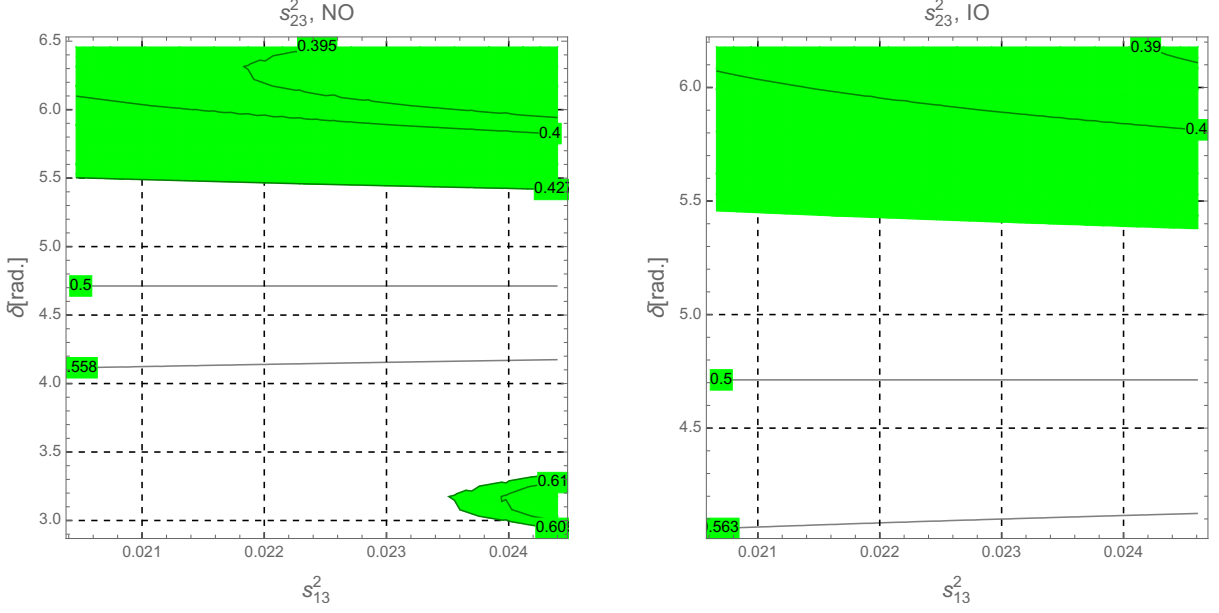


FIG. 2: Contour plots for s_{23}^2 as a function of s_{13}^2 and δ for the NO and IO schemes. The green regions are excluded by 3σ data of s_{23}^2 . The black curves show the constant values of s_{23}^2 .

by identifying that $e^{ix} = e^{iy}$ is equivalent with $x = y$ without the unnecessary repeated term $k2\pi$, $k \in \mathbb{Z}$. Hence, the non-zero contribution to the Majorana phase is

$$\gamma_3 = \delta - \phi_0, \quad (28)$$

consistent with the result mentioned in Ref. [10].

From now on, three parameters θ_{12} , θ_{23} , and ϕ_0 will be written as functions of s_{13} and δ based on the relations given in Eqs. (22), (23), (24), and (25). Taking these functions for diagonalisation m_ν by requiring that $[U_1^T m'_\nu U_1]_{13} = 0$ will lead to $s_{2\theta} [(m'_\nu)_{33} e^{i\phi_0} - (m'_\nu)_{11} e^{-i\phi_0}] = 2(m'_\nu)_{13} c_{2\theta}$, where $(m'_\nu)_{11}$, $(m'_\nu)_{13}$, and $(m'_\nu)_{33}$ are given in Eq. (19). The result is

$$t_{2\theta} \equiv \tan(2\theta) = \frac{2(m'_\nu)_{13}}{(m'_\nu)_{33} e^{i\phi_0} - (m'_\nu)_{11} e^{-i\phi_0}}, \quad (29)$$

leading to the following exact solution of $\tilde{\epsilon}$,

$$\begin{aligned} \tilde{\epsilon} &= \frac{\sqrt{E} - 6it_{2\theta}\tilde{\kappa}^{-1}\sin(\phi_0) + 4t_{2\theta}\cos(\phi_0) - 4\sqrt{3}}{4(t_{2\theta}\cos(\phi_0) + \sqrt{3})}, \\ E &= 8t_{2\theta} \left(t_{2\theta}\cos(\phi_0) + \sqrt{3} \right) \left((9\tilde{\kappa}^{-2} + 4)\cos(\phi_0) - 12i\tilde{\kappa}^{-1}\sin(\phi_0) \right) \\ &\quad + \left(6it_{2\theta}\tilde{\kappa}^{-1}\sin(\phi_0) - 4t_{2\theta}\cos(\phi_0) + 4\sqrt{3} \right)^2. \end{aligned} \quad (30)$$

Here, we choose $\tilde{\epsilon}$ guarantees that $\lim_{t_{2\theta} \rightarrow 0} \tilde{\epsilon} = 0$, consistent with our assumption that $\theta = 0$ results in the TB form of U_{PMNS} . We note that formula of $\tilde{\epsilon}$ is more general than that given in the original SS models [11, 26], where $\tilde{\epsilon}$ was assumed to be small for the approximate solutions. The Majorana phases defined in Eq. (17) are also formulated based on the phases of $U_1^T m'_\nu U_1$. Then, the more precise form of U_{PMNS} defined in Eq. (12) is

$$U_{\text{PMNS}} \equiv U_{\text{PMNS}}^0 \text{diag} \left(1, e^{\frac{i\alpha_{21}}{2}}, e^{\frac{i\alpha_{31}}{2}} \right), \quad (31)$$

$$\begin{aligned} \alpha_{21} &= \text{Arg}[(m'_\nu)_{11} c_\theta^2 - (m'_\nu)_{13} s_{2\theta} e^{i\phi_0} + (m'_\nu)_{33} s_\theta^2 e^{2i\phi_0}] - \text{Arg}[(m'_\nu)_{22}] \text{ [Deg.],} \\ \alpha_{31} &= \text{Arg}[(m'_\nu)_{11} c_\theta^2 - (m'_\nu)_{13} s_{2\theta} e^{i\phi_0} + (m'_\nu)_{33} s_\theta^2 e^{2i\phi_0}] \\ &\quad - \text{Arg}[(m'_\nu)_{33} c_\theta^2 + (m'_\nu)_{13} s_{2\theta} e^{-i\phi_0} + (m'_\nu)_{11} s_\theta^2 e^{-2i\phi_0}] + \gamma_3 \text{ [Deg.],} \end{aligned} \quad (32)$$

where γ_3 is given in Eq. (28) contributes to the phase α_{31} , apart from those come from the phases of the neutrino masses in the diagonal matrix $U_1^T m'_\nu U_1$.

At this step, all of the active neutrino masses and mixing parameters can be formulated in terms of the five independent parameters s_{13} , δ , m_0 , ϕ_1 , and κ . Until now, we do not know the orders of m_0 and κ , hence it is necessary to take some numerical estimation to figure out these orders.

The definition $\Delta m_{ij}^2 \equiv m_{n_i}^2 - m_{n_j}^2$ gives

$$\begin{aligned} \frac{\Delta m_{21}^2}{m_0^2} &= \frac{16}{|\kappa^2(2 + \tilde{\epsilon})^2|^2} - |(m'_\nu)_{11} c_\theta^2 - (m'_\nu)_{13} s_{2\theta} e^{i\phi_0} + (m'_\nu)_{11} s_\theta^2 e^{2i\phi_0}|^2, \\ \frac{\Delta m_{32}^2}{m_0^2} &= |(m'_\nu)_{33} c_\theta^2 + (m'_\nu)_{13} s_{2\theta} e^{-i\phi_0} + (m'_\nu)_{11} s_\theta^2 e^{-2i\phi_0}| - \frac{16}{|\kappa^2(2 + \tilde{\epsilon})^2|^2}. \end{aligned} \quad (33)$$

As a result, Δm_{32}^2 is written as a function of Δm_{21}^2 and $\tilde{\kappa} = \kappa e^{i\phi_1}$ for both NO and IO schemes. The experimental data of s_{ij} , Δm_{21}^2 , Δm_{32}^2 , and δ will give constraints on κ and ϕ_1 . In the TB limit, the right-hand sides of Eqs. in (33) depend only on κ and ϕ_1 . The condition $\Delta m_{21}^2 > 0$ requires $\kappa < 1.6$ being useful for estimating the deviation of $(\tilde{\rho} - \tilde{\kappa})$ to looking for a real mixing angle s_{13} .

For the first estimation of κ and ϕ_1 with $\tilde{\epsilon} \neq 0$, we find numerically that $\Delta m_{21}^2/m_0^2$ depend weakly on s_{13}^2 . Therefore, it is fixed at the best-fit point when $\Delta m_{21}^2/m_0^2$ is plotted as a function of κ and ϕ_1 in the range $0 \leq \phi_1 \leq 360$ [Deg.], while δ is chosen at some typical values in the allowed range 141 [Deg.] $< \delta < 340$ [Deg.] for both NO and IO schemes. Adding a requirement that the formula of $\Delta m_{21}^2/m_0^2$ given in Eq. (33) must be positive, values of $\kappa > 1.9$ are excluded, see the numerical illustrations in Fig. 3. The allowed regions

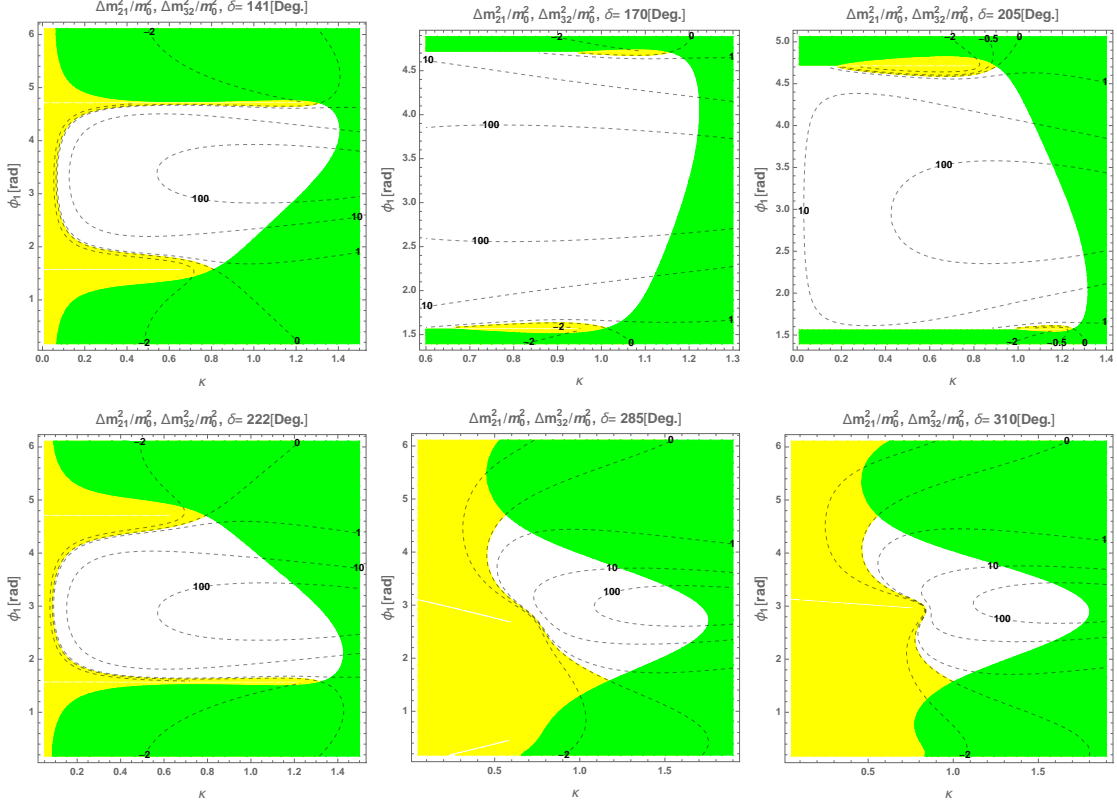


FIG. 3: $\Delta m_{21}^2/m_0^2$ and $\Delta m_{32}^2/m_0^2$ as functions of κ and ϕ_1 with different δ and s_{13}^2 at the best-fit point. The green regions are excluded by the requirement $\Delta m_{21}^2/m_0^2 > 0$. The yellow regions correspond to $\Delta m_{21}^2/m_0^2 \leq 0$. The dashed black curves show the constant values of $\Delta m_{32}^2/m_0^2$.

of $\{\kappa, \phi_1\}$ depend rather complicatedly on δ . In Fig. 3, the contour plot of $\Delta m_{32}^2/m_0^2$ are also shown, where the two yellow and non-color regions supporting the respective IO and NO schemes are separated by the constant curve $\Delta m_{32}^2/m_0^2 = 0$. It can be estimated that, the allowed regions for the NO scheme always require that $1.4 \times 180/\pi < \phi_1 < 4.8 \times 180/\pi$ [Deg].

More details for the NO scheme, we require that $R_{32,21} \equiv \Delta m_{32}^2/\Delta m_{21}^2$ derived from Eq. (33) must in the allowed experimental range

$$R_{32,21} \in \left[\frac{\min^{\text{exp}}(\Delta m_{32}^2)}{\max^{\text{exp}}(\Delta m_{21}^2)} \simeq 29.4, \frac{\max^{\text{exp}}(\Delta m_{32}^2)}{\min^{\text{exp}}(\Delta m_{21}^2)} \simeq 37.5 \right]. \quad (34)$$

Now, from numerical illustrations shown in Fig. 4, the allowed regions (blue) are more constrained. We also add here the contour plots of m_0 as a function of ϕ_1 and κ given in Eq. (33) and Δm_{21}^2 is fixed at the best-fit point. The numerical investigation above shows that for the NO scheme, κ must satisfies $0.4 < \kappa < 1.6$. And the order of m_0 is around

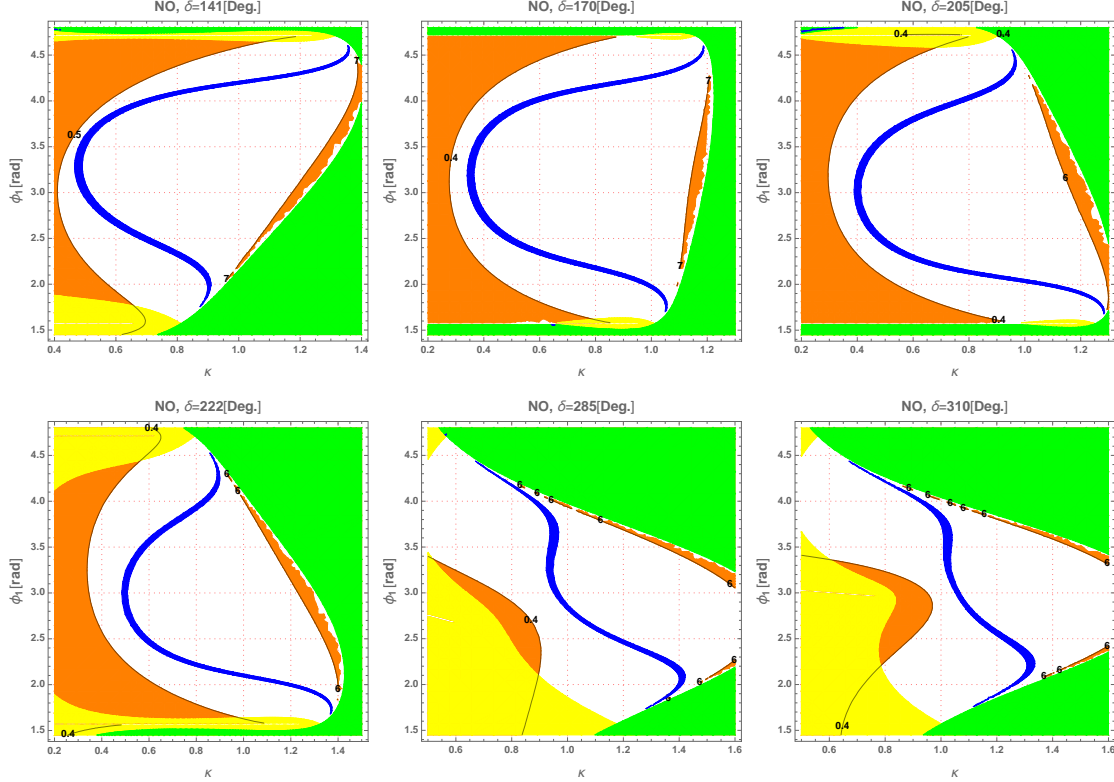


FIG. 4: Contour plots of $R_{32,21}$ and m_0 as functions of κ and ϕ_1 in the NO case with fixed s_{13}^2 at best-fit point and different δ . The blue regions satisfy the condition in Eq. (34). The yellow regions and green regions are the same as those in Fig. 3. The two black curves show constant values $x_{1,2}$ of $m_0 \times 10^{11} [\text{GeV}]$ and separate the non color region having m_0 in the range $x_1 < m_0 < x_2$ with the orange regions out side this range.

10^{-10} eV. In addition, every allowed ϕ_1 corresponds to a very narrow allowed range of κ . Regarding the IO scheme, the allowed regions are very narrow for fixed δ values, and require that ϕ_1 must be in the two ranges $[0, 90]$ and $[270, 360]$ [Deg.]. In addition, the allowed ranges of κ and m_0 are similar to those from the NO scheme, hence will be used to scan for determining more general allowed regions in the following numerical investigation.

B. Low energy observables

As we discussed above, the neutrino mass matrix in Eq. (19) depends on the set of five free real parameters $(s_{13}, \delta, \phi_1, \kappa, m_0)$ used to scan numerically. By fixing s_{13} , δ , and Δm_{21}^2 , we have estimated the reasonable ranges of all parameters m_0 , κ , and ϕ_1 . They will be

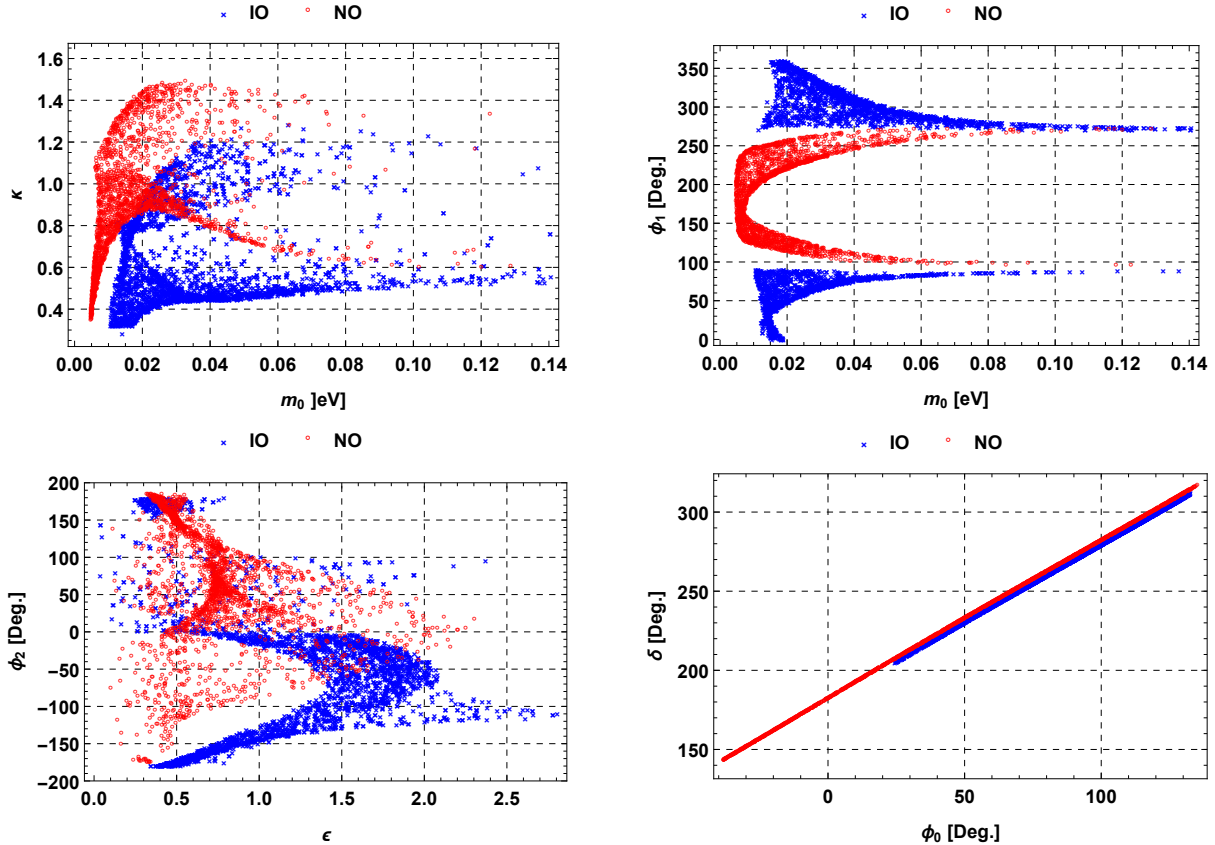


FIG. 5: The allowed ranges of the parameters appearing in the model under consideration.

used to scan all five independent parameters ($s_{13}, \delta, m_0, \kappa, \phi_1$) to collect all allowed points satisfying the 3σ experimental data in the general case. For both NO and IO schemes, the unknown parameters get random values in the following ranges:

$$0.001 \text{ eV} \leq m_0 \leq 0.18 \text{ eV}, \quad 0.05 \leq \kappa \leq 1.65, \quad 0 \leq \phi_1 < 2\pi \text{ [rad.]}, \quad (35)$$

and the two parameters s_{13} and δ runs over 3σ allowed range of the experimental data. We stress that wider ranges of m_0 and κ were investigated before choosing the best ranges for the following numerical illustration. The parameter spaces ($\kappa, \epsilon, \phi_0, \phi_1, \phi_2 = \arg[\tilde{\epsilon}]$) and their correlations are respectively plotted in Fig. 5, where the red and the blue patterns represent the allowed regions predicted by the NO and the IO schemes, respectively. Hereafter, we continue using these conventions if there is no more explanation. We note that the upper bound values of m_0 for the typical NO (IO) scheme was estimated from our numerical investigation. We can find that the allowed regions of the model's parameters are separated completely for the two schemes. In particular, the ranges $0.35 < \kappa < 1.5$, $0.1 < \epsilon < 2.3$, $-40 < \phi_0 < 140$ [Deg.], $90 < \phi_1 < 270$ [Deg.], $-180 < \phi_2 < 180$ [Deg.] support the NO

scheme while the IO implies the allowed values of the parameters as $0.3 < \kappa < 1.3$, $0 < \epsilon < 3$, $25 < \phi_0 < 135$ [Deg.], $(0 < \phi_1 < 90) \cup (270 < \phi_1 < 360)$ [Deg.], $-180 < \phi_2 < 180$ [Deg.]. The predicted ranges for the CP phase δ in the two schemes are more narrow than the respective 3σ experimental data, namely $141 < \delta < 320$ [Deg.] for the NO and $205 < \delta < 310$ [Deg.] for the IO. The lower bounds of δ are matched with that of experimental bounds for both cases of neutrino mass hierarchy. Whereas, the upper bounds of δ are lower than about 50 [Deg.] comparing with their experimental values as given in Eqs. (15) and (16).

The light neutrino masses predicted by the model are respectively plotted in Fig. 6 as function of the light neutrino mass scale m_0 for the NO (left panel) and the IO (right panel). There the red, blue, green plots represent for m_1, m_2, m_3 , respectively. We can recognize that the neutrino masses are strong hierarchy with small values of m_0 and they can be quasi degenerate $m_1 \cong m_2 \cong m_3 \geq 0.12$ eV for both hierarchies if m_0 approaching about 0.12 eV.

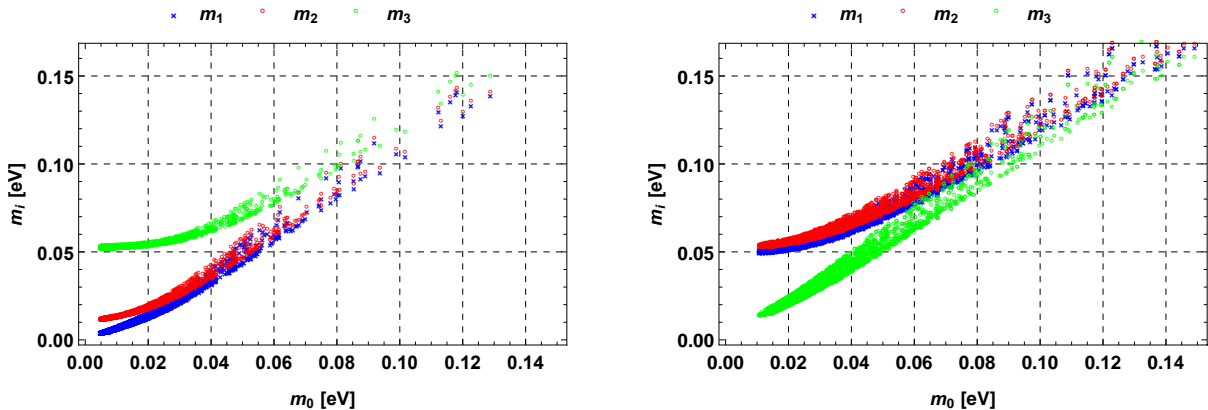


FIG. 6: The active neutrino masses m_i as functions of m_0 in the left (right) panel predicted by the NO (IO) scheme.

We all know that neutrino oscillation experiments could not determine the absolute scale of active neutrino masses. Instead, it can be measured by non-oscillation neutrino experiment such as Tritium beta decay [63], neutrinoless double beta decay ($0\nu\beta\beta$) [64], or by cosmological and astrophysical observations [65]. As the model consequences, we would like to study the effective neutrino masses associate with $0\nu\beta\beta$ ($|\langle m \rangle|$) and beta decay (m_β) which are defined as

$$|\langle m \rangle| = \left| \sum_{i=1}^3 m_i (U_{\text{PMNS}})_{ei}^2 \right| = \left| \left(m_1 c_{12}^2 + m_2 s_{12}^2 e^{i\alpha_{21}} \right) c_{13}^2 + m_3 s_{13}^2 e^{i(\alpha_{31} - 2\delta)} \right|, \quad (36)$$

$$m_\beta = \sqrt{\sum_{i=1}^3 m_i^2 |(U_{\text{PMNS}})_{ei}|^2} = \sqrt{m_1^2 c_{13}^2 c_{12}^2 + m_2^2 c_{13}^2 s_{12}^2 + m_3^2 s_{13}^2}. \quad (37)$$

In Eq. (36), we can use directly $U_{3\nu}$ given in Eq. (17) instead of U_{PMNS} defined in Eq. (31). The predictions of the allowed regions presenting the relation between effective masses $|\langle m \rangle|$ and m_β with the lightest active neutrino mass, m_{lt} , are respectively plotted in Fig. 7 and Fig. 8 (left panel). Whereas, the correlation between m_β and $|\langle m \rangle|$ is shown in the right panel of the Fig. 8.

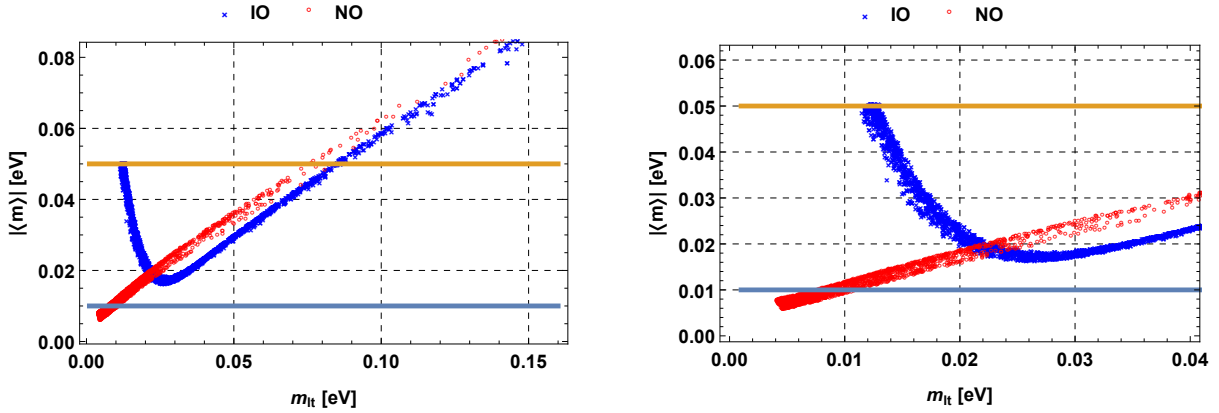


FIG. 7: The relations between $|\langle m \rangle|$ with the lightest mass m_{lt} . The solid horizontal lines are the sensitivities of $|\langle m \rangle|$ of the new generation of neutrinoless double beta decay experiment [66].

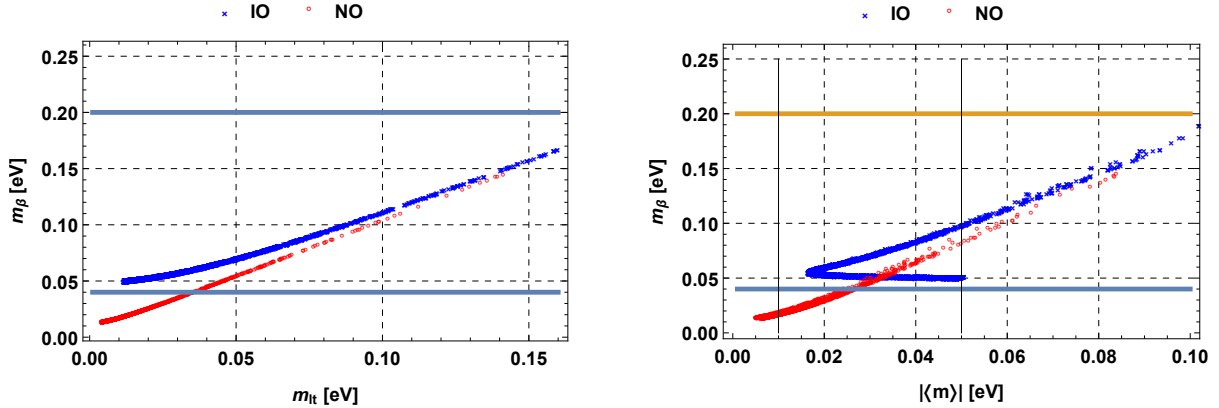


FIG. 8: The relations between m_β with m_{lt} ($|\langle m \rangle|$) in the left (right) panel. The solid horizontal lines are the prospect sensitivities of Katrin (0.2 eV) [67] and Project 8 (0.04 eV) [68]. The solid vertical lines are the sensitivities of $|\langle m \rangle|$ of the new generation of neutrinoless double beta decay experiment [66].

The consequence is that the IO scheme is excluded for $m_\beta < 0.05$ eV, or $|\langle m \rangle| < 0.015$

eV. In contrast, the NO is excluded for $m_\beta < 0.01$ eV or $|\langle m \rangle| < 0.005$ eV. In addition, the sharpened allowed regions in the right panel of Fig. 8 implies the very strict relations between m_β and $|\langle m \rangle|$ for both schemes. On the other word, the model is very predictive. Because once both of these quantities are observed, the reality of the model is immediately confirmed. If it survive, based on the two separated regions corresponding the NO and IO schemes, the model can figure out only one of the two schemes survive.

III. THE HIGGS SECTOR

The same as the SM, the covariant derivative for local $SU(2)_L \otimes U(1)_Y$ symmetry is

$$D_\mu = \partial_\mu - igT^a W_\mu^a - i\frac{g'}{2}B_\mu Y. \quad (38)$$

Here T^a ($a = 1, 2, 3$) are the generators of the $SU(2)_L$ symmetry. The kinetic terms of the two Higgs doublets generating gauge boson masses are:

$$\mathcal{L}_{\text{kin}}^H = (D_\mu h_u)^\dagger (D^\mu h_u) + (D_\mu h_d)^\dagger (D^\mu h_d). \quad (39)$$

The SM charged gauge bosons are $W^\pm \equiv (W^1 \mp iW^2)/\sqrt{2}$. The same relation known in two Higgs doublet models (2HDMs) for the two vevs,

$$v^2 = v_u^2 + v_d^2 = 174^2 \text{GeV}^2, \quad t_W = \frac{s_W}{c_W} \equiv \frac{g'}{g}, \quad (40)$$

where $s_W^2 = 0.231$. The model also contains the SM Z boson satisfying $W_\mu^3 = c_W Z_\mu + s_W A_\mu$ and $B_\mu = -s_W Z_\mu + c_W A_\mu$.

A detailed analytical calculation on the mass and mixing of the Higgs in the 2HDMs was done previously, for example in Ref. [69]. Similarly to the very important parameter t_β defined by the ratio of the two neutral Higgs VEVs in the MSSM and the 2HDM, t_β in the model under consideration is defined as follows:

$$t_\beta \equiv \tan \beta = \frac{v_u}{v_d}. \quad (41)$$

It is noted that from now on we will use the following conventions for any angles $x = \delta, \alpha, \beta, 2\alpha, 2\beta$, and $(\beta - \alpha)$: $t_x \equiv \tan(x)$, $s_x \equiv \sin(x)$, $c_x \equiv \cos(x)$. Because the Yukawa couplings of charged leptons with h_d in Eq. (3) is fixed, t_β defined in this model is consistent with Refs. [51, 70], but equivalent to $1/t_\beta$ defined in other MSSM and 2HDMs discussed previously.

For the Higgs spectrum, this model must contain at least one SM-like Higgs boson observed by the LHC. It is one of those included in the squared mass matrix of the CP-even Higgs boson, which is a 10×10 matrix consisting of a large number of the independent Higgs self-couplings. In this work, we will choose a simple case of the realistic Higgs potential, which is summarized in the appendix B. Here we will focus on the identification of SM-like Higgs boson. In particular, a simple regime is chosen that these Higgs doublets decouple to other Higgs singlets, and a soft term generate masses for CP-odd neutral Higgs and results in heavy charged Higgs bosons, the same as those appear in the well-known 2HDM [53].

The model contains two singly charged Higgs bosons φ^\pm and two massless states G_W^\pm which are Goldstone bosons eaten by gauge bosons W^\pm . The masses and relations between the original and physical states of the charged Higgs components are:

$$m_{G_W}^2 = 0, \quad m_\varphi^2 = \left(\lambda_4 v^2 + \frac{\mu_{12}^2}{s_\beta c_\beta} \right),$$

$$H_u^\pm = s_\beta G_W^\pm + c_\beta \varphi^\pm, \quad H_d^\pm = -c_\beta G_W^\pm + s_\beta \varphi^\pm. \quad (42)$$

Regarding CP-odd neutral Higgs components, the squared mass matrix has a zero determinant, which implies exactly a massless state corresponding to the Goldstone boson of the Z boson in the SM. One of the remaining CP-odd neutral Higgs boson relate to the two Higgs doublets with mass satisfying $m_A^2 = \frac{\mu_{12}^2}{s_\beta c_\beta} = m_\varphi^2 - \lambda_4 v^2$, implying that $\mu_{12}^2 > 0$.

For the CP-even neutral Higgs corresponding to the simple case we assume above, the total squared mass matrix will separate into two submatrices, namely a 2×2 and a 8×8 ones. The 8×8 matrix gives eight physical heavy Higgs bosons with masses depending on heavy VEVs v_S and v_T , see appendix B for the details. In the original basis $(S_u, S_d)^T$ given in Eq. (1), the 2×2 matrix containing the SM-like Higgs boson has the following form,

$$\mathcal{M}^2 = \begin{pmatrix} 2\lambda_1 v_u^2 + \mu_{12}^2 t_\beta^{-1} & 2\lambda_3 v_u v_d - \mu_{12}^2 \\ 2\lambda_3 v_u v_d - \mu_{12}^2 & 2\lambda_2 v_d^2 + \mu_{12}^2 t_\beta \end{pmatrix}. \quad (43)$$

It gives two mass eigenstates, denoted as H and h_1 where the lighter $h_1 \equiv h$ will be identified with the SM-like Higgs boson. Their masses and relations with the original states are

$$m_{H,h}^2 = \frac{1}{2} \left[\mathcal{M}_{11}^2 + \mathcal{M}_{22}^2 \pm \sqrt{(\mathcal{M}_{11}^2 - \mathcal{M}_{22}^2)^2 + 4(\mathcal{M}_{12}^2)^2} \right],$$

$$S_u = c_\alpha h + s_\alpha H, \quad S_d = -s_\alpha h + c_\alpha H. \quad (44)$$

where α is defined based on the following relation

$$t_{2\alpha} \equiv \tan 2\alpha = -\frac{2t_\beta [m_\varphi^2 - (2\lambda_3 + \lambda_4)v^2]}{(m_\varphi^2 - \lambda_4 v^2)(t_\beta^2 - 1) + 2(\lambda_2 - \lambda_1 t_\beta^2)v^2}. \quad (45)$$

Because the SM-like Higgs boson h were found experimentally at LHC, we require that the its couplings with normal fermions and gauge bosons have small deviations with those predicted by the SM, see the Feynman rules given in table II. Here all quarks multiplets

TABLE II: Couplings of the SM-like Higgs with SM particles $H_1 \equiv h$

Vertex	Coupling	Vertex	Coupling
$h\bar{e}_a e_a$	$\frac{igm_{e_a} s_\alpha}{2m_W c_\beta}$	$h\bar{q}_a q_a$	$\frac{igm_{q_a} s_\alpha}{2m_W c_\beta}$
$hW_\mu^+ W_\nu^-$	$igm_W \sin(\beta - \alpha)g^{\mu\nu}$	$hZ_\mu Z_\nu$	$\frac{igm_W}{c_W^2} \sin(\beta - \alpha)g^{\mu\nu}$

are assumed to be singlets under all A_4 and other discrete symmetries listed in table I. The Yukawa Lagrangian of quark is

$$-\mathcal{L}_q^Y = y_{ab}^d \overline{Q}_{aL} h_d d_{bR} + y_{ab}^u \overline{Q}_{aL} \tilde{h}_d u_{bR} + h.c., \quad (46)$$

where $\tilde{h}_d = i\sigma_2 h_d^* = (v_d + \frac{S_d - iA_d}{\sqrt{2}}, -H_d^-)^T$. Correspondingly, the top quark mass is $m_t = v_d y_t$, leading to the perturbative limit $m_t/v_d = y_t < \sqrt{4\pi}$. As a result, we have $c_\beta = v_d/v > m_t/(v\sqrt{4\pi})$, equivalently $t_\beta \leq 3.4$. The model now treats like the 2HDM type-I, which the recent constraints on the model parameters were given in Ref. [55, 57]. The typical constraints on the free parameters are $|s_\delta| \leq 0.05$ and $t_\beta \leq 3.3$.

There is another assignment of quark sector corresponds to the case of the 2HDM type-II and the MSSM: all upper quarks only couple with h_u , leading to the condition $t_\beta \geq 0.3$ for the perturbative limit. The recent constraints of the model parameters were given in Refs. [54, 57], where the typical ranges of free parameters are $|s_\delta| < 0.008$ and $0.2 \leq t_\beta \leq 5$ after casting into the model under consideration. The Lagrangian contains Yukawa couplings of quarks with charged Higgs boson is:

$$\mathcal{L}_{ud\varphi} = -\frac{g}{\sqrt{2}m_W} V_{ab}^* \bar{d}_b (t_\beta m_{d_b} P_L + t_\beta^{-1} m_{u_b} P_R) u_a \varphi^- + \text{H.c.}, \quad (47)$$

where V is the Caibibbo-Cobayashi-Maskawa matrix, m_{q_a} with $q = u, d$ and $i = 1, 2, 3$ is the mass of the quark q_a .

We note that t_β defined in this work is equivalent with $1/t_\beta$ defined in Ref. [54, 55] for both type-I and II of the 2HDM. Our numerical calculation does not depend on the

assignments of quark, except the $\mu - e$ conversion rate, which was discussed for the MSSM, including the contributions from the charged Higgs bosons in the 2HDM type II. But the phenomenology investigated in this work strongly depend on t_β , leading to another channel to determine which $SU(2)_L$ Higgs doublet generates quark masses.

From the recent experimental data, the coupling of the SM-like boson with normal charged leptons, namely $h\bar{e}_a e_a$ given in Table II, must be consistent with the coupling predicted from in the SM, leading to a consequence that $s_\alpha \simeq -c_\beta$. A small deviation from the SM couplings correspond to a small parameter δ satisfying

$$\sin(\beta - \alpha) \equiv \cos \delta \simeq 1, \quad (48)$$

equivalently $\delta \equiv \frac{\pi}{2} + \alpha - \beta \simeq 0$, which is known in the 2HDMs. The constraints of δ , t_β , and charged Higgs bosons comes from the electroweak and Higgs precision measurements discussed recently for the 2HDMs [54, 55, 58],

In conclusion, in the numerical investigation, the free parameters in the Higgs sector we will use are β , δ , $m_h \equiv m_h$, m_φ , λ_2 , and λ_4 . The SM-like Higgs mass $m_h \equiv m_h \simeq 125.09$ GeV was determined experimentally from LHC. Three parameters α and $\lambda_{1,3}$ are determined from three Eqs. (48), (44), and (45). We are interesting in the regions allowing large range of t_β , hence we will fix $\lambda_4 = 0$, and $m_A = m_{H_2} = m_\varphi$, which were shown from previous discussions [55–57]. Based on the general formulas of the three parameters $\lambda_{1,2,3}$ given in Ref. [69], they can be written as follows:

$$\begin{aligned} \lambda_1 &= \frac{c_\alpha^2 m_h^2 + m_\varphi^2 (s_\alpha^2 - c_\beta^2)}{2v^2 s_\beta^2}, \quad \lambda_2 = \frac{s_\alpha^2 m_h^2 + m_\varphi^2 (c_\alpha^2 - s_\beta^2)}{2v^2 s_\beta^2}, \\ \lambda_3 &= \frac{-s_\alpha c_\alpha m_h^2 + m_\varphi^2 (s_\beta c_\beta + s_\alpha c_\alpha)}{2v^2 c_\beta s_\beta}. \end{aligned} \quad (49)$$

The analytic formulas of these three Higgs self couplings will be used to calculate the coupling $h\varphi^+\varphi^-$ that contributes to the LFVHD.

IV. LFV DECAYS

A. Neutrino sector: ISS relations vs the exact numerical solution

In this section we study effects of the allowed regions of parameter space on the LFV decays. The neutrino mixing is the only source of the LFV processes. The original basis

of the nine left-handed neutral neutrinos are denoted as $\nu'_L = (\nu_L, (N_R)^c, (X_R)^c)^T$, where $\psi_L \equiv (\psi_{1L}, \psi_{2L}, \psi_{3L})^T$, for all all leptons $\psi_L \equiv \nu_L, (N_R)^c, (X_R)^c$. Also, the original right-handed neutrino basis is $\nu'_R = (\nu'_L)^c = ((\nu_L)^c, N_R, X_R)^T$ with $\psi_R = (\nu_{aL})^c, N_{aR}, X_{aR}$. A four-component spinor for a Majorana neutrino is then $\psi = (\psi_L, \psi_R)^T$ where $\psi = \nu_a, N_a, X_a$ satisfying $\psi^c = C\bar{\psi}^T = \psi$, where C is the charge conjugation operator. The relations between a four-component Majorana spinor with the respective left- and right-handed components are $\psi_{L,R} = (\psi_{R,L})^c = P_{L,R}\psi$, where $P_{L,R} = (1 \mp \gamma_5)/2$. The mass term of these nine neutrinos were given in two Eqs. (2) and (3). The corresponding mass matrix is diagonalized by a total 9×9 unitary mixing matrix U^ν determined as follows:

$$U^{\nu T} \mathcal{M}^\nu U^\nu = \hat{\mathcal{M}}^\nu = \text{diag}(m_{n_1}, m_{n_2}, \dots, m_{n_9}) = \text{diag}(m_1, m_2, m_3, M_1, M_2, \dots, M_6), \quad (50)$$

where the first three masses m_{n_a} ($a = 1, 2, 3$) and respective eigenvectors n_a are identified with those of active neutrinos observed by experiments defined in Eq. (10). The remaining ones belong to those of the six heavy neutrinos n_{I+3} with $I = 1, 2, \dots, 6$. Relations between original and mass neutrino bases are

$$\nu'_{iL} = U_{ij}^\nu n_{jL} = U_{ij}^\nu P_L n_j, \quad \text{and} \quad \nu'_{iR} = U_{ij}^{\nu*} n_{jR} = U_{ij}^{\nu*} P_R n_j, \quad (51)$$

where $n = (n_1, n_2, \dots, n_9)^T$ and $n_i = (n_{iL}, n_{iR})^T$ ($i = 1, 2, \dots, 9$). The matrix U^ν is parameterized as follows [34, 71, 72],

$$U^\nu = \exp \begin{pmatrix} \mathbf{O} & R \\ -R^\dagger & \mathbf{O} \end{pmatrix} \begin{pmatrix} U_{3\nu} & \mathbf{O} \\ \mathbf{O} & V_6 \end{pmatrix}, \quad (52)$$

where \mathbf{O} is the 3×3 matrix with all elements being zeros, V_6 is the unitary matrix, $\exp(x) \equiv \sum_{i=0}^{\infty} x^i/i!$, and R is the 3×6 matrix satisfying the ISS condition that $\max|R_{ai}| \ll 1$ for all $a = 1, 2, 3$ and $i = 1, 2, \dots, 9$. Accordingly, the ISS relations given in Eq. (9) are obtained from the expansion U^ν up to the order $\mathcal{O}(R^2)$. Correspondingly, the sub-matrix R and heavy neutrino masses in this case are

$$R^* \simeq (-m_D^T M^{-1}, \quad m_D^T M_R^{-1}),$$

$$V_6^* \hat{M}_N V_6^\dagger = M_N + \frac{1}{2} R^T R^* M_N + M_N \frac{1}{2} R^\dagger R, \quad M_N \equiv \begin{pmatrix} 0 & M_R^T \\ M_R & \mu_X \end{pmatrix}, \quad (53)$$

where $M \equiv M_R^T \mu_X^{-1} M_R$ and $\hat{M}_N \simeq \text{diag}(M_1, M_2, \dots, M_6)$ presents six heavy neutrino masses.

Before determining Feynman rules to calculate Br of LFV decays, we remark some requirements to guarantee the ISS relations given in Eqs. (9) and (53). In principle, in order to be consistent between the approximation solution from the ISS relations and the exact one obtained directly from calculating numerically the total neutrino mass matrix given in Eq. (5), the condition $\max(|R_{ai}|) \ll 1$ must satisfy, equivalently $\max(|m_D(M_R^T)^{-1}|_{ai}) \ll 1$, leading to a consequence that the two scales $v_u f$ and M_0 given in (7) must satisfy $v_u f/M_0 \ll 1$.

Direct numerical calculation to derive masses and mixing of the active neutrino from the total neutrino mass \mathcal{M}^ν , it is necessary to know the input as the following set of free parameters $\{m_d, M_0, \mu_X, \tilde{\kappa}, \tilde{\rho}\}$. We limit our investigation in the allowed regions of the parameter space indicated in section II B. Namely, two parameters $\tilde{\kappa}$ and $\tilde{\rho}$ reduce to two allowed values of κ and ϕ_1 . The parameter μ_X is considered as a function of m_0 from Eq. (20), then allowed values of m_0 can be determined from the numerical investigation. These allowed values will be used as the inputs. The remaining parameters $m_D \equiv v f$, and M_0 do not appear in the approximate solution of active neutrino data using ISS relation (10) because it is absorbed in m_0 . Instead, the constraint of m_0 is used to determine μ_X . In contrast, determining \mathcal{M}^ν requires all of the three parameters. In numerical investigation, the exact solution is found by using the software mathematica 11 to find the mixing matrix U^ν relating with the eigenvectors of the matrix $\mathcal{M}^{\nu\dagger}\mathcal{M}^\nu$ and the neutrino masses.

B. Feynman rules for LFV decays

In the Yukawa Lagrangian parts (2) and (3), couplings relating to LFV decays are

$$-\mathcal{L} \rightarrow \frac{m_{e_a}}{\sqrt{2}v_d} S_d \bar{e}_a e_a + \frac{m_{e_a}}{v_d} (\bar{\nu}_{La} e_{aR} H_d^+ + \text{H.c.}) + \frac{S_u}{\sqrt{2}} f (\bar{\nu}_{aL} N_{aR} + \text{H.c.}) + f [H_u^- \bar{e}_{aL} N_{aR} + \text{H.c.}],$$

where the third term results in the coupling $h\bar{n}_i n_j$ for the ISS mechanism discussed in detail in Ref. [35, 73]. We can prove that

$$f\bar{\nu}_{aL} N_{Ra} = \frac{1}{v_u} \bar{n}_i (D_{ij}^* m_{n_j} P_R) n_j, \quad D_{ij} \equiv \sum_{a=1}^3 U_{ai}^{\nu*} U_{aj}^\nu, \quad (54)$$

which was introduced firstly in Ref. [35]. Using the definition $\lambda_{ij} \equiv (D_{ij} m_{n_i} + D_{ij}^* m_{n_j})$ needed to write the right Feynman rules for Majorana neutral lepton in terms of Dirac

spinors [33, 36, 72], the coupling $h\bar{n}_i n_j$ is written in the symmetric form as follows:

$$\frac{gc_\alpha}{4s_\beta m_W} h \sum_{i,j=1}^9 \bar{n}_i (\lambda_{ij} P_L + \lambda_{ij}^* P_R) n_j.$$

In the unitary gauge, the Feynman rules for vertex couplings relating with the decay processes in this work are given in table III, consistent with those mentioned in the 2HDMs [53].

TABLE III: Feynman rules for couplings contributing to LFV decays, $\Gamma = s_\beta c_\beta (c_\alpha c_\beta \lambda_1 - s_\alpha s_\beta \lambda_2) + (c_\alpha s_\beta^3 - s_\alpha c_\beta^3) \lambda_3 + \sin(\beta - \alpha) \lambda_4$

Vertex	Coupling	Vertex	Coupling
$\bar{e}_a e_a h$	$-\frac{igm_{e_a}}{2m_W} (c_\delta - t_\beta s_\delta)$	$h\varphi^+ \varphi^-$	$-\frac{2im_W}{g} \Gamma$
$\bar{n}_i n_j h$	$-\frac{ig}{2m_W} (c_\delta + t_\beta^{-1} s_\delta) (\lambda_{ij} P_L + \lambda_{ij}^* P_R)$	$hW_\mu^+ W_\nu^-$	$igm_W c_\delta g^{\mu\nu}$
$\bar{e}_a n_i \varphi^-$	$\frac{-igU_{ai}^\nu}{m_W \sqrt{2}} (m_{e_a} t_\beta P_L + m_{n_i} t_\beta^{-1} P_R)$	$\bar{n}_i e_a \varphi^+$	$\frac{-igU_{ai}^{\nu*}}{m_W \sqrt{2}} (m_{e_a} t_\beta P_R + m_{n_i} t_\beta^{-1} P_L)$
$h\varphi^+ W_\mu^-$	$\frac{igs_\delta}{2} (p_h - p_{\varphi^+})^\mu$	$h\varphi^- W_\mu^+$	$\frac{-igs_\delta}{2} (p_h - p_{\varphi^-})^\mu$
$\bar{e}_a n_i W_\mu^-$	$\frac{ig}{\sqrt{2}} U_{ai}^\nu \gamma^\mu P_L$	$\bar{n}_i e_a W_\mu^+$	$\frac{ig}{\sqrt{2}} U_{ai}^{\nu*} \gamma^\mu P_L$

C. LFV decays $e_b \rightarrow e_a \gamma$

In the limit $m_a^2/m_b^2 \ll 1$, $m_{a,b}$ being masses of charged leptons e, μ and τ , the Brs of the cLFV decays $e_b \rightarrow e_a \gamma$ is determined as follows [74, 75],

$$\text{Br}(e_b \rightarrow e_a \gamma) = \frac{3\alpha_e}{2\pi} \left(|D_{(ba)L}|^2 + |D_{(ba)R}|^2 \right) \times \text{Br}(e_b \rightarrow e_a \bar{\nu}_a \nu_b), \quad (55)$$

where $D_{(ba)L,R}$ are scalar factors arising from loop corrections, $\alpha_e \simeq 1/137$ in numerical investigations, and the experimental values of the $\text{Br}(e_b \rightarrow e_a \bar{\nu}_a \nu_b)$ are $\text{Br}(\tau \rightarrow \mu \bar{\nu}_\mu \nu_\tau) \simeq 17.41\%$, $\text{Br}(\tau \rightarrow e \bar{\nu}_e \nu_\tau) \simeq 17.83\%$ and $\text{Br}(\mu \rightarrow e \bar{\nu}_e \nu_\mu) \simeq 100\%$. The analytic expressions $D_{(ba)L,R} = D_{(ba)L,R}^W + D_{(ba)L,R}^\varphi$ are determined in Appendix C. The one loop contributions were established the same way as those mentioned in the SS case [26], and consistent with [74, 75]. The two loop contributions mentioned in the 2HDM type-X model given in Ref. [76] do not appear in our model.

D. Decays $\mu \rightarrow eee^+ \equiv \mu \rightarrow 3e$.

The analytic formulas base on the analytical results for non-supersymmetric contributions to LFV decays in the 2HDM presented in Refs. [48, 51, 52], and results Refs. [77–79] which general formulas can be used for the 2HDM. The μ - e conversion rate for the ISS model were given in Ref. [50]. The partial decay width $\mu \rightarrow 3e$ is taken from Ref. [51], namely only the non-supersymmetric contributions are collected. The decay rate is

$$\begin{aligned} \text{Br}(\mu \rightarrow 3e) = & \left\{ 2 \left| \frac{1}{2} F_{\text{box}}^{\mu e e e, LL} + F_Z^{\mu e, L} - 2s_W^2 \left(F_Z^{\mu e, L} - F_\gamma^{\mu e, L} \right) \right|^2 + 4s_W^4 \left| F_Z^{\mu e, L} - F_\gamma^{\mu e, L} \right|^2 \right. \\ & + 16s_W^2 \text{Re} \left[\left(F_Z^{\mu e, L} + \frac{1}{2} F_{\text{box}}^{\mu e e e, LL} \right) G_\gamma^{\mu e, L*} \right] - 48s_W^4 \text{Re} \left[\left(F_Z^{\mu e, L} - F_\gamma^{\mu e, L} \right) G_\gamma^{\mu e, L*} \right] \\ & \left. + 32s_W^4 |G_\gamma^{\mu e, L}|^2 \left[\ln \frac{m_\mu^2}{m_e^2} - \frac{11}{4} \right] \right\} \times \frac{\pi \alpha_W^2}{64}, \end{aligned} \quad (56)$$

where $\Gamma_\mu = \alpha_W^2 m_\mu^5 / (384\pi m_W^4)$, $\alpha_W = g^2 / (4\pi)$, and the loop functions are listed in the appendix C. In the limit of the ISS model, the Eq. (56) is consistent with that given in Refs. [48, 49]. Apart from the gauge boson and Higgs contributions taken from Refs. [48, 49], the Higgs contributions were checked with the results given in Refs. [80, 81].

E. $\mu - e$ conversion in nuclei

Based on the results given in Refs. [48, 51, 70], we collect all one-loop non-supersymmetric contributions to the $\mu - e$ conversion rates, see the detailed formulas listed in appendix C. In the model under consideration the $\mu - e$ conversion rate $R_{\mu \rightarrow e}^J$ in a nuclei J consisting of Z protons and N neutrons is

$$R(J) \equiv R_{\mu \rightarrow e}^J = \frac{G_F^2 \alpha_W^2 \alpha^3 m_\mu^5}{8\pi^4 \Gamma_{\text{capt}}} \times \frac{Z_{\text{eff}}^4}{Z} F_p^2 \left(|Q_W^L|^2 + |Q_W^R|^2 \right), \quad (57)$$

where $Q_W^X = (2Z + N)V_u^X + (Z + 2N)V_d^X$, $X = L, R$. $V_{u,d}^L$ is defined as follows

$$\begin{aligned} V_q^L &= Q_q s_W^2 \left(F_{\gamma, \mu e}^L + G_{\gamma, \mu e}^R \right) + F_{Z, \mu e}^L \left(\frac{1}{2} I_q^3 - Q_q s_W^2 \right) + \frac{1}{4} F_{\text{Box}}^{\mu e q q}, \quad q = u, d, \\ V_q^R &= Q_q s_W^2 \left(F_{\gamma, \mu e}^R + \frac{m_e}{m_\mu} G_{\gamma, \mu e}^L \right) + F_{Z, \mu e}^R \left(\frac{1}{2} I_q^3 - Q_q s_W^2 \right), \end{aligned} \quad (58)$$

where Q_q and I_3 are the electric charge and iso spin of the quark $q = u, d$. To determine V_q^X with $X = L, R$, we just consider the limit of the 2HDM type II so that the couplings

of the charged Higgs bosons with all quarks in our model are the same as those given in Ref. [51]. Well-known values of Z_{eff} , F_p , and Γ_{capt} corresponding to various nuclei are given in table IV [48, 82]. The form factors $F_{\gamma,\mu e}^X$, $F_{Z,\mu e}^X$, $G_{\gamma,\mu e}^X$, and $F_{\text{box}}^{\mu e q q}$ are collected in

TABLE IV: Effective atomic charges, nuclear form factors and capture rates, $N = A - Z$.

${}^A_Z J$	Z_{eff}	$F_p(-m_\mu^2)$	$\Gamma_{capt}(10^6 s^{-1})$ [10^{-18} GeV]	$R_{\mu \rightarrow e}^J$ (current bound)	$R_{\mu \rightarrow e}^J$ (future sensitivity)
${}^{17}_{13}\text{Al}$	11.5	0.64	0.7054 [0.4641]		$10^{-16} - 10^{-17}$
${}^{48}_{22}\text{Ti}$	17.6	0.54	2.59 [1.7042]	$\leq 4.3 \times 10^{-12}$	10^{-18}
${}^{197}_{79}\text{Au}$	33.5	0.16	13.07 [8.5987]	$\leq 7 \times 10^{-13}$	
${}^{208}_{82}\text{Pb}$	34.0	0.15	13.45 [8.8487]	$\leq 4.3 \times 10^{-11}$	

appendix C.

F. LFV decays of the SM-like Higgs boson $h \rightarrow e_a e_b$

In the unitary gauge, the Feynman diagrams corresponding to one-loop contributions to the LFV decay amplitudes of the SM-like Higgs boson $h \rightarrow e_a e_b$ are shown in Fig. 9. The

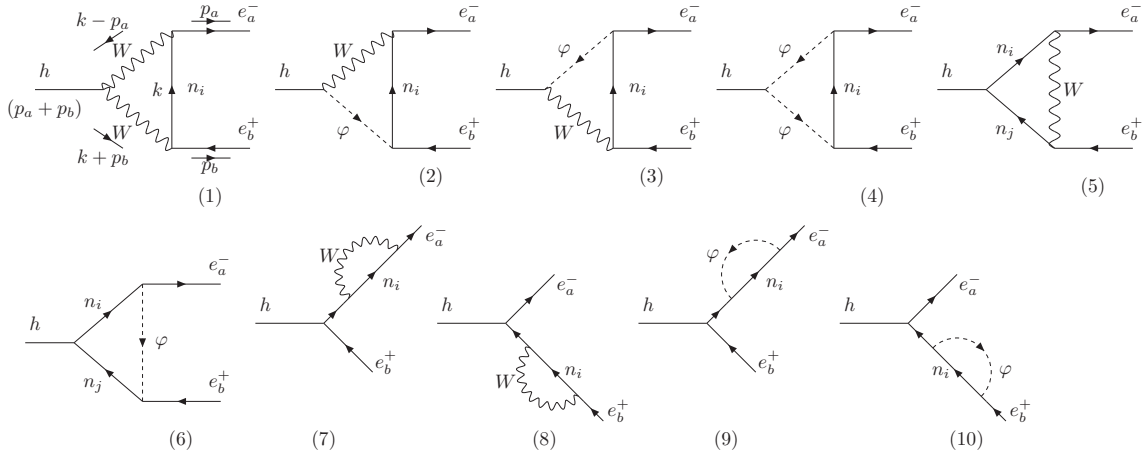


FIG. 9: One-loop Feynman diagrams for $h \rightarrow e_a e_b$ in the unitary gauge.

effective Lagrangian of the decay is written as $\mathcal{L}^{\text{LFV}h} = h (\Delta_L \bar{e}_a P_L e_b + \Delta_R \bar{e}_a P_R e_b) + \text{H.c.}$, where $\Delta_{(ba)L,R}$ are scalar factors arising from the loop contributions. The partial width of the decay is

$$\Gamma(h \rightarrow e_a e_b) \equiv \Gamma(h \rightarrow e_a^- e_b^+) + \Gamma(h \rightarrow e_a^+ e_b^-) = \frac{m_h}{8\pi} (|\Delta_{(ba)L}|^2 + |\Delta_{(ba)R}|^2), \quad (59)$$

with the condition $m_h^2 \gg m_{a,b}^2$. The LFVHD decay rate is $\text{Br}(h \rightarrow e_a e_b) = \Gamma(h \rightarrow e_a e_b) / \Gamma_h^{\text{total}}$ where $\Gamma_h^{\text{total}} \simeq 4.1 \times 10^{-3}$ GeV is the SM value. The deviation of Γ_h^{total} from SM is small with $|s_\delta| \leq 0.05$ defined in Eq. (48), hence we can ignore this change in our numerical investigation. In notations constructed in [83], the $\Delta_{(ba)L,R}$ can be written as

$$\Delta_{(ba)L,R} = \sum_{i=1}^{10} \Delta_{(ba)L,R}^{(i)}, \quad (60)$$

where $\Delta_{(ba)L,R}^{(i)}$ is listed in the Appendix D. Detailed calculations are based on [83], where modifications have been made in appendix D to make the Passarino-Veltman (PV) functions to be consistent with LoopTools. In the SM limit given by Eq. (48), formulas relating contributions from only W boson are consistent with those shown in [37] calculated in the unitary gauge, and consistent with previous analytic formulas performed in the 't Hooft-Feynman gauge [33].

V. NUMERICAL INVESTIGATION OF LFV DECAYS

A. Setup parameters

In this section we will apply the allowed regions of the parameter space mentioned above to investigate the LFV decays. First, we discuss the independent parameters needed to determine numerically the masses and mixing matrix of all neutrinos from the total mass matrix given in Eq (5). The five independent parameters s_{13} , δ , ϕ_1 , κ and m_0 will be constrained from the experimental data, as we have presented precisely. In exact numerical calculation using the direct neutrino mass matrix (5), more unknown parameters are $m_D \equiv v f$, t_β , and M_0 .

Apart from the free parameters mentioned above, there are unknown parameters relating with the Higgs sector. In particular, contributions of charged Higgs bosons φ^\pm depends on m_φ , the mixing angle δ between the CP-even neutral Higgs bosons, and four Higgs-self couplings $\lambda_{1,2,3,4}$ in coupling factor $h\varphi^+\varphi^-$. But all of them are not independent and we can choose the new independent parameters are m_h , m_φ , and δ as we discussed previously. The perturbative constraints for these Higgs self-couplings of the model are [54, 69, 84]:

$$0 < \lambda_{1,2}, \quad |\lambda_3| < 4\pi, \quad \lambda_3 + \sqrt{\lambda_1 \lambda_2} > 0, \quad \lambda_3 + \sqrt{\lambda_1 \lambda_2} > 0. \quad (61)$$

We fix $m_h = 125.09$ GeV. The Dirac mass scale $m_D = vf < 174 \times \sqrt{4\pi} \simeq 616$ GeV. The heavy neutrino masses are originated from the A_4 breaking scale M_0 hence they can be very large. This situation is completely different from that discussed previously in Refs. [36], where heavy neutrino masses are bounded from above because of the Casas-Ibarra parametrization [34] specializing the structure of Dirac mass term m_D , resulting in the perturbative limit of the Yukawa coupling. In the numerical investigation, we require $M_0/(m_D s_\beta) \geq 10 \gg 1$, necessary to obtain the consistent ISS relations given in Eqs. (9) and (53).

Discussions on the lower bounds of the charged Higgs boson in 2HDMs were discussed on Ref. [85]. Constraints on the $\varphi^\pm \rightarrow \gamma W^\pm$ decay and the STU parameters [86]. Recent experimental data of charged Higgs decays $\varphi^+ \rightarrow \bar{q}q', \bar{\ell}\nu_\ell$ [87]. The model has non zero coupling $hW^\pm\varphi^\mp$, which predicts a decay $\varphi^\pm \rightarrow hW^\pm$ having $\Gamma(\varphi^\pm \rightarrow hW^\pm) \sim \sin^2 \delta$. In the alignment limit, $\delta \rightarrow 0$, this decay channel vanishes. When $0 \neq \delta \ll 1$, the recent experimental constraint must be considered. A global fit on the 2HDM was discussed on Ref. [88].

For the case of the 2HDM type-II, based on the recent results given in Ref. [54], the allowed regions of parameters for $m_\varphi \leq 2$ TeV are: $0.2 \leq t_\beta \leq 5$, $|s_\delta| \leq 0.008$, $\lambda_4 v < 200$ GeV. On the other hand, in the case of $\lambda_4 = 0$ and $s_\delta \rightarrow 0$, the values of t_β is relaxed to a large values of $t_\beta \sim 50$. In the study on the parameter space corresponding more heavy masses of the Higgs bosons [57], the large t_β values are still allowed. For the case of the 2HDM type-I, based on the recent results given in Ref. [55], the allowed regions of parameters are: $t_\beta < 3$, $|s_\delta| \leq 0.05$, $\lambda_4 v < 200$ GeV.

In the numerical investigation for studying the LFV phenomenology using the allowed values of the set $\{s_{13}, \delta, m_0, \kappa, \phi_1\}$ that obtained from scanning the ranges given in Eq. (35), the remaining unknown parameters as follows. For the cLFV processes, related unknown parameters are m_D , M_0 , and t_β , which do not depend on the quark couplings, i.e. independent with which type-I or II of the 2HDM. While parameter space of the model under consideration are constrained by recent experimental data of $\text{Br}(\mu \rightarrow \gamma)$ and $\text{Br}(\mu \rightarrow 3e)$, the two other decay rates $\text{Br}(\tau \rightarrow \mu\gamma, e\gamma)$ seem much smaller. The interesting possibility is they may be large enough to be detected by the future experimental sensitivities of the order $\mathcal{O}(10^{-9})$. By collecting only points that satisfy all of the conditions $10^{-14} \leq \text{Br}(\mu \rightarrow e\gamma) < 4.2 \times 10^{-13}$, $\text{Br}(\mu \rightarrow 3e) < 10^{-12}$, and $\max[\log[\text{Br}(\tau \rightarrow \mu\gamma)], \log[\text{Br}(\tau \rightarrow e\gamma)]]$ is as large as possible, we

find a requirement that $m_D \geq \mathcal{O}(1)$ GeV which will be paid attention to in the following discussion. The unknown parameters are scanned in the following ranges

$$100 \text{ GeV} \leq m_D \leq 600 \text{ GeV}, \quad 10 \leq \frac{M_0}{m_D s_\beta} \leq 100,$$

$$0.02 \leq t_\beta \leq 50, \quad 700 \text{ GeV} \leq m_\varphi \leq 10^4 \text{ GeV}, \quad (62)$$

where the second constraint bases on the ISS condition (53), namely $|R_{ai}| \ll 1$ for all $a = 1, 2, 3, i = 1, 2, \dots, 6$.

To looking for regions of the parameter space allows large $\text{Br}(h_1^0 \rightarrow \tau\mu, \tau e)$ and satisfy the constraints $\text{Br}(\mu \rightarrow e\gamma) < 4.2 \times 10^{-13}$ and $\text{Br}(\mu \rightarrow 3e) < 10^{-12}$, we need to scan s_δ in the range $|s_\delta| \leq 0.05$ (0.008) for model type-I (II) and adding a requirement given in Eq. (61). We note that the small ranges of m_D GeV were scanned but they give suppressed values of $\text{Br}(h_1^0 \rightarrow e_a e_b)$. In the numerical investigation, we just collect points satisfying $\max[\text{Br}(h_1^0 \rightarrow \mu\tau, e\tau)] \geq 10^{-11}$.

To discuss on the μ -e conversion rates predicted by the 2HDM type-II only the following allowed range of t_β is considered: $0.3 \leq t_\beta \leq 50$. The most interesting allowed range $0.2 \leq t_\beta \leq 5$ given in Ref. [54] will also be remarked.

B. Numerical results

1. LFVHD and cLFV processes

The correlation between $\text{Br}(h_1^0 \rightarrow e_a e_b)$ and $\text{Br}(\mu \rightarrow e\gamma)$ are plotted in the Fig. 10 for the NO scheme. Only points satisfying both conditions $\text{Br}(\mu \rightarrow e\gamma) < 4.2 \times 10^{-13}$ and $\max[\text{Br}(h_1^0 \rightarrow e_a e_b)] \geq 10^{-11}$ are collected. The similar results are found for the IO scheme, hence we will not show here. Correspondingly, largest values of LFVHD is the $\text{Br}(h_1^0 \rightarrow \tau\mu)$ satisfying $10^{-10} \leq \max[\text{Br}(h_1^0 \rightarrow \tau\mu)] < 10^{-9}$, but $\text{Br}(h_1^0 \rightarrow \tau e) \leq 10^{-11}$. Both schemes always result in suppressed values of $\text{Br}(h_1^0 \rightarrow \mu e)$, hence it will not be discussed. The regions corresponding to the current constraint of $\text{Br}(\mu \rightarrow e\gamma)$ give largest values of LFVHD satisfying $\text{Br}(h_1^0 \rightarrow \tau\mu) \leq \mathcal{O}(10^{-10})$, and $\text{Br}(h_1^0 \rightarrow \tau e) \leq \mathcal{O}(10^{-11})$. These values are much smaller than the values $\mathcal{O}(10^{-7})$ predicted previously by other models with ISS neutrinos where LFVHD arises from loop corrections. These difference can be explained by the particular parameterization the total neutrino mass matrix. In the model under

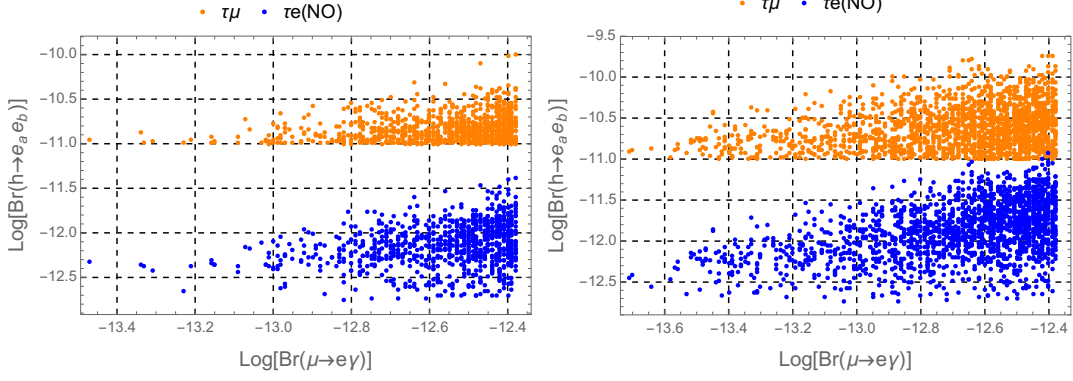


FIG. 10: The correlation between LfVHD vs. $\text{Br}(\mu \rightarrow e\gamma)$ in the NO scheme corresponding two ranges $0.02 \leq t_\beta \leq 3.4$ (left) and $0.3 \leq t_\beta \leq 50$ (right).

consideration, the A_4 symmetry results in a very strict structure of the total neutrino mass matrix, which is the origin of the very strict relations between the cLFV and LfVHD decays.

We continue with the numerical results for the cLFV decays $\text{Br}(e_b \rightarrow X)$ with $\{e_b, X\} = \{\tau, \mu\gamma\}, \{\tau, e\gamma\}, \{\mu, 3e\}$. The results are shown in Fig. 11 for the NO schemes. The similar

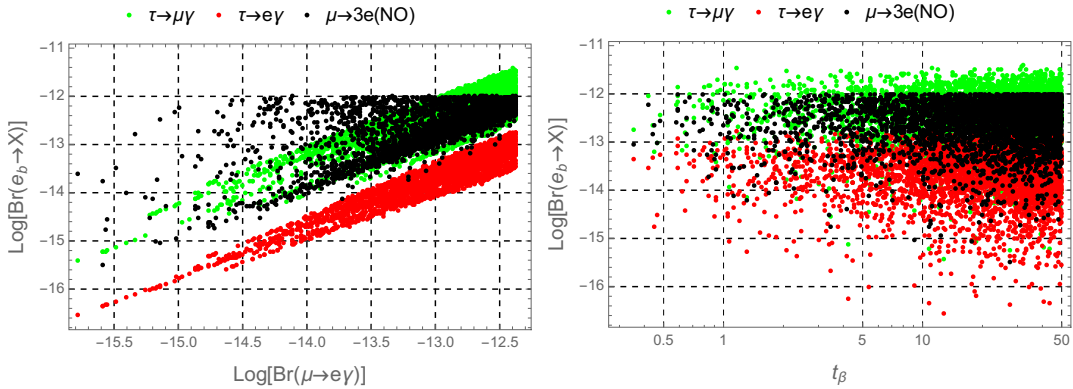


FIG. 11: cLFV rates as functions of $\text{Br}(\mu \rightarrow e\gamma)$ (t_β) in the left (right) panel for the NO scheme.

results are found for the IO scheme, see Fig. 12. The common property for both schemes is that the constraints of $\text{Br}(\mu \rightarrow e\gamma)$ and $\text{Br}(\mu \rightarrow 3e)$ affect strongly on the two decays $\text{Br}(\tau \rightarrow \mu\gamma, e\gamma)$, leading to the following upper bounds $\text{Br}(\tau \rightarrow \mu\gamma) < 10^{-11}$ and $\text{Br}(\tau \rightarrow e\gamma) < 10^{-12}$ (10^{-13}) for the NO (IO) scheme.

In conclusion for the cLFV decays, we find that $\text{Br}(\tau \rightarrow \mu\gamma, e\gamma)$ can reach the order $\mathcal{O}(10^{-11})$, much larger than $\text{Br}(\mu \rightarrow e\gamma)$. But they can not large enough to be observed by experiments with planned sensitivities of $\mathcal{O}(10^{-9})$. Our conclusion for the LfVHD and cLFV decays are completely different from the results predicted by the 2HDM type III,

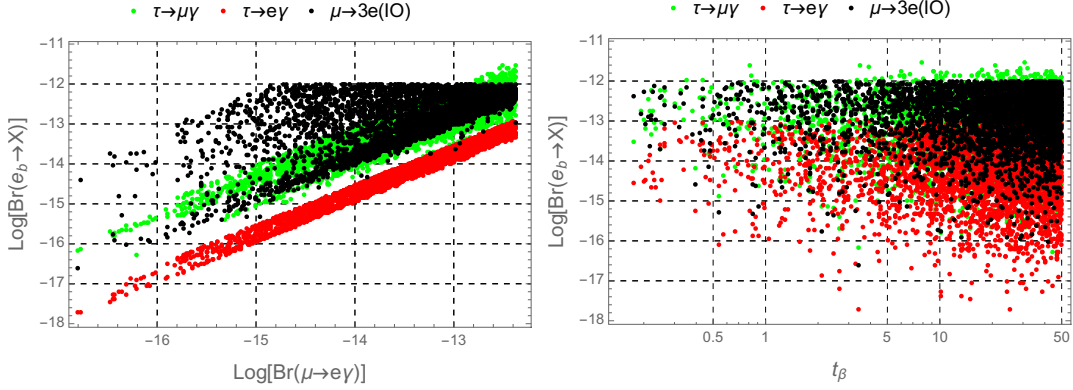


FIG. 12: cLFV rates as functions of $\text{Br}(\mu \rightarrow e\gamma)$ (t_β) in the left (right) panel for IO scheme.

where LFBVHD appears at tree level and does not depend on the constraint of $\text{Br}(\mu \rightarrow e\gamma)$ [76, 89, 90].

2. μ - e conversions in nuclei predicted by the 2HDM type-II.

Regarding to the μ - e conversion corresponding to the 2HDM type-II, with $0.3 \leq t_\beta \leq 50$. The correlations between $\text{Br}(\mu \rightarrow e\gamma)$ and the four μ - e conversions rates are shown precisely in Fig. 13. All μ - e conversion rates are constrained strictly by the data of the decay $\mu \rightarrow \gamma$.

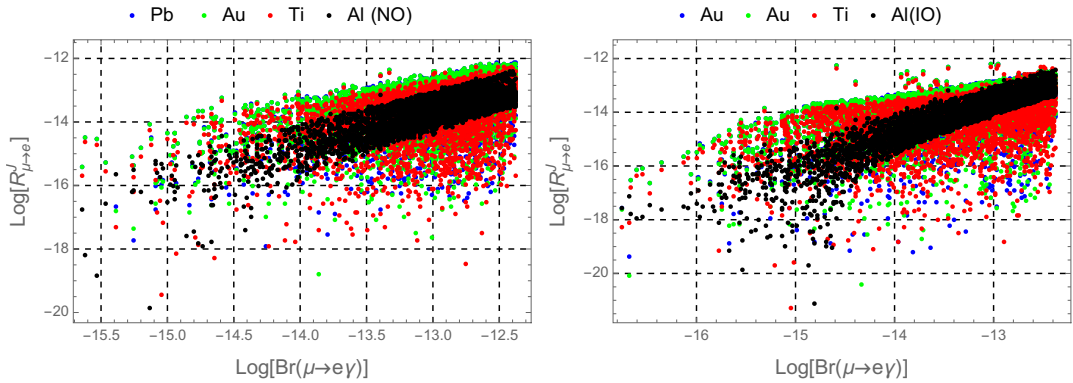


FIG. 13: Correlations between $\log[\text{Br}(\mu \rightarrow 3e)]$ and different μ - e conversion rates for $0.3 \leq t_\beta \leq 50$.

They decrease with smaller $\text{Br}(\mu \rightarrow \gamma)$. The allowed regions corresponding to the three nuclei Ti, Au, and Pb are nearly the same, while the allowed region for Al is more narrow. The recent constraint of $\text{Br}(\mu \rightarrow e\gamma)$ gives an upper bound of 10^{-12} for all μ - e conversions rates. The planned sensitivity of 6×10^{-14} can give the upper bound of 10^{-13} .

The results in this case for both NO and IO schemes are nearly the same, hence we just

consider the NO scheme in the below discussion. The allowed regions of the parameter space does not changes significantly with t_β and m_φ . On the other hand, these regions change for different μ -e conversion rates. Their shapes are the same with m_D and M_0 . The dependence of μ -e rates on m_D is shown in Fig. 14 for the NO scheme. The allowed regions of $R(Al)$ are

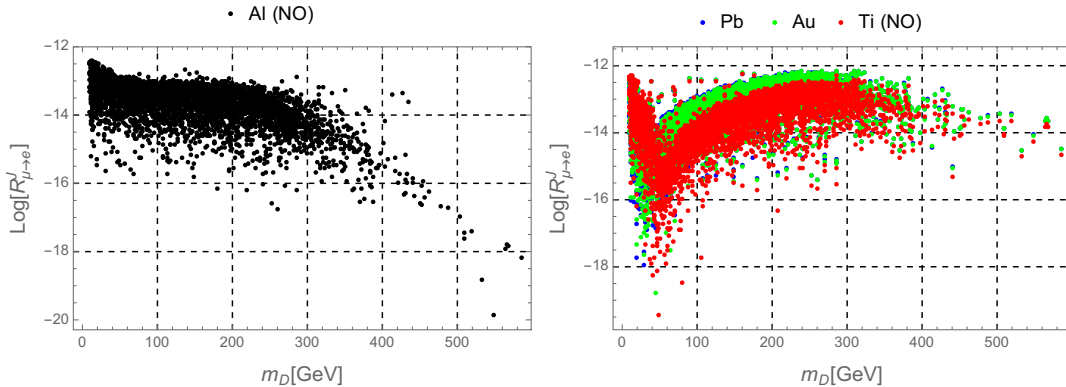


FIG. 14: Correlations between m_D and different μ -e conversion rates.

different from the remaining conversion rates because of $Z - N$ is positive for Al, in contrast with the three remaining nuclei. Hence the combining the μ -e results conversion rates will give more strict values of m_D .

Finally, we remind that the above allowed regions of parameters satisfy the recent experimental bound $(\mu \rightarrow 3e) < 10^{-12}$. If this channel is not observed with planned sensitivity of 10^{-16} , the upper bounds of cLFV decays and or μ -e conversion rates will be more suppressed, see illustration in Fig. 15 for the NO scheme, where correlations between $\text{Br}(\mu \rightarrow 3e)$ and

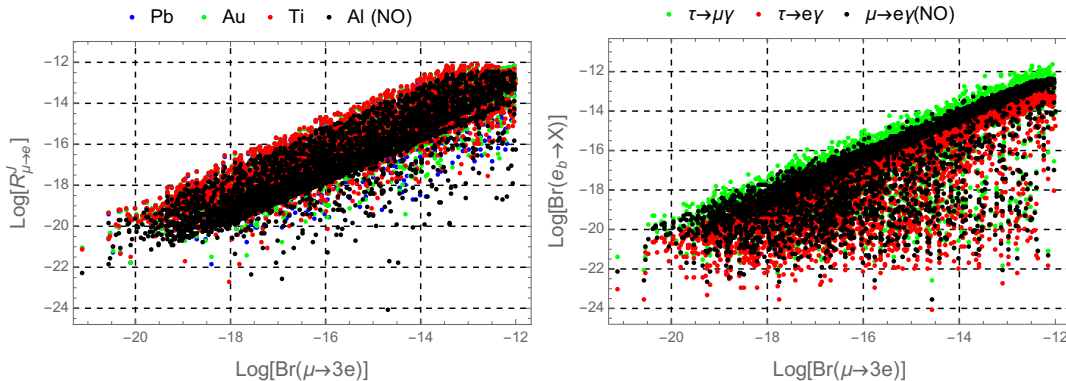


FIG. 15: Correlations between $\log[\text{Br}(\mu \rightarrow 3e)]$ and different μ -e conversion rates (cLFV rates) in the left (right) panel.

other cLFV decays the four μ -e conversions rates are shown precisely. The new ranges

of m_D and M_0 are $10^{-2} \text{ GeV} \leq m_D \leq 600 \text{ GeV}$ and $10 \leq \frac{M_0}{m_D s_\beta} \leq 10^3$. The respective constraints of the cLFV and μ -e conversion rates are: $\text{Br}(\tau \rightarrow \mu\gamma)$, $R(J) \leq 10^{-15}$, and $\text{Br}(\tau, \mu \rightarrow e\gamma) \leq 10^{-16}$. In other word, planned experimental upper bound of $\text{Br}(\mu \rightarrow 3e)$ predicts more strict upper bounds of $\text{Br}(e_b \rightarrow e_a\gamma)$ than those from the respective experimental sensitivities.

VI. CONCLUSION

In this work, we have introduced the A_4 ISS model to explain the recent experimental data of neutrino oscillation. The total neutrino mass matrix arises from the A_4 symmetry, resulting in the ISS form of the active neutrino mass matrix. All masses and mixing parameters of the active neutrino corresponding to the oscillation data were formulated as functions of five independent parameters: $(s_{13}, \delta, \phi_1, \kappa, m_0)$. We have determined all allowed ranges of these parameters satisfying 3σ experimental neutrino oscillation data. From this, the model predicts the two following ranges of the m_β and $\langle m \rangle$ and the following: i) $0.01 \text{ eV} \leq m_\beta \leq 0.15 \text{ eV}$ and $0.005 \text{ eV} \leq |\langle m \rangle| \leq 0.09 \text{ eV}$ for the NO scheme, ii) $0.05 \text{ eV} \leq m_\beta \leq 0.17 \text{ eV}$ and $0.015 \text{ eV} \leq |\langle m \rangle| \leq 0.1 \text{ eV}$ for IO scheme. These ranges can be observed by the forthcoming experiments. More interesting, the two allowed regions of these two quantities predicted by the two NO and IO schemes shown in the right panel of Fig. 8 are very narrow and nearly distinguishable. As a result, this A_4 ISS model will predict which IO or NO schemes is realistic or the model is ruled out, once both quantities m_β and $|\langle m \rangle|$ are observed by upcoming experiments.

The active and heavy ISS neutrinos in the A_4 ISS model result in cLFV and μ -e conversion nuclei from loop corrections. Numerical results indicated that $\text{Br}(\mu \rightarrow e\gamma, 3e)$ give strong upper bounds on other cLFV decays and μ -e conversion rates. The recent experimental constraints of $\text{Br}(\mu \rightarrow e\gamma, 3e)$ result in the very suppressed decay rates of $\text{Br}(h \rightarrow e_a e_b) < \mathcal{O}(10^{-9})$ and $\text{Br}(\tau \rightarrow \mu\gamma, e\gamma) < 10^{-11}$, which are much smaller than the planned experimental sensitivities. In the other side, the μ -e conversion rates still reach the orders $\mathcal{O}(10^{-12})$, which is in the observable ranges of experiments. The planned sensitivity of $\text{Br}(\mu \rightarrow 3e) \sim \mathcal{O}(10^{-16})$ gives much stronger constraints on the cLFV processes that can not be observed, including $\text{Br}(\mu \rightarrow e\gamma) < 10^{-16}$. The promising signals now are the μ -e conversion rates of Al and Ti. In conclusion, the A_4 ISS we introduced here is very predictive.

The reality of the model and many interesting predictions on the observable quantities such as m_β , $|\langle m \rangle|$, cLFV decay rates, and μ -e conversion rates in nuclei will be confirmed or ruled out by the upcoming experiments.

Acknowledgments

This research is funded by Vietnam National Foundation for Science and Technology Development (NAFOSTED) under grant number 103.01-2018.331. L. T. Hue is thankful to Van Lang University.

Appendix A: A_4 group in the AF (Altarelli-Feruglio) basis

The non-Abelian A_4 is a group of even permutations of 4 objects and has $4!/2 = 12$ elements, see a review in [91–93]. The group is generated by two generators S and T satisfying the relations $S^2 = (ST)^3 = (T^3) = 1$. The group has four irreducible representations (rep.), including three one-dimensional and one three-dimensional ones which are denoted as $\underline{1}$, $\underline{1}'$, $\underline{1}''$, and $\underline{3}$, respectively. The multiplication rules for them are as follows

$$\begin{aligned} \underline{1} \times \underline{R} &= \underline{R} \times \underline{1} = \underline{R}, \quad \underline{1}' \times \underline{1}'' = \underline{1}, \quad \underline{1}' \times \underline{1}' = \underline{1}'', \quad \underline{1}'' \times \underline{1}'' = \underline{1}', \\ \underline{3} \times \underline{3} &= \underline{3} + \underline{3}_A + \underline{1} + \underline{1}' + \underline{1}'', \end{aligned} \quad (\text{A1})$$

where $\underline{3}$ and $\underline{3}_A$ imply the symmetric and anti-symmetric forms of the respective Clebsch-Gordan coefficients, which particular formulas depend on the choice of T and S . In this work, the three-dimensional unitary representations of T and S are [94, 95]. Correspondingly, the Clebsch-Gordan coefficients obtained from tensor products of the two A_4 triplets $a = (a_1, a_2, a_3)$ and $b = (b_1, b_2, b_3) \sim \underline{3}$ are

$$\begin{aligned} \underline{1} &\equiv (ab)_{\underline{1}} = (a_1b_1 + a_2b_3 + a_3b_2), \\ \underline{1}' &\equiv (ab)_{\underline{1}'} = (a_3b_3 + a_1b_2 + a_2b_1), \\ \underline{1}'' &\equiv (ab)_{\underline{1}''} = (a_2b_2 + a_1b_3 + a_3b_1), \\ \underline{3} &\equiv (ab)_{\underline{3}} = \frac{1}{3}(2a_1b_1 - a_2b_3 - a_3b_2, 2a_3b_3 - a_1b_2 - a_2b_1, 2a_2b_2 - a_1b_3 - a_3b_1), \\ \underline{3}_A &\equiv (ab)_{\underline{3}_A} = \frac{1}{2}(a_2b_3 - a_3b_2, a_1b_2 - a_2b_1, a_3b_1 - a_1b_3). \end{aligned} \quad (\text{A2})$$

Only rep. $\underline{3}$ is used for generating the neutrino mass matrix. In the mentioned basis, \mathbb{T} is complex and $T^* \neq T$ in general so the complex conjugate representation r^* of a representation r ($r = \underline{1}'$, $\underline{1}''$, $\underline{3}$) is not the same as r , although they are all real reps.. It is determined by the following rules [94, 95]: $c \sim \underline{1} \rightarrow c^* \sim \underline{1}$, $c' \sim \underline{1}' \rightarrow c'^* \sim \underline{1}'^* = \underline{1}''$, $c'' \sim \underline{1}' \rightarrow c''^* \sim \underline{1}''^* = \underline{1}'$, and $a = (a_1, a_2, a_3) \sim \underline{3} \rightarrow a^* = (a_1^*, a_3^*, a_2^*) \sim \underline{3}$.

Appendix B: The total Higgs potential

The Higgs potential respecting all symmetries given in table I is

$$\begin{aligned}
V_{Higgs} = & \mu_u^2 h_u^\dagger h_u + \mu_d^2 h_d^\dagger h_d + \frac{\lambda_1}{2} (h_u^\dagger h_u)^2 + \frac{\lambda_2}{2} (h_d^\dagger h_d)^2 + \lambda_3 (h_d^\dagger h_d) (h_u^\dagger h_u) \\
& + \lambda_4 (h_d^\dagger h_u) (h_u^\dagger h_d) + \left\{ \mu_{ud}^2 (i\sigma_2 h_u)^T h_d + \text{h.c.} \right\} + \sum_{x=u,d} \sum_H \lambda^{xH} (h_x^\dagger h_x) (H^\dagger H)_1 \\
& + \mu_{\xi'}^2 \xi'^\dagger \xi' + \mu_{\xi''}^2 \xi''^\dagger \xi'' + \lambda^{\xi' \xi''} (\xi' \xi'') (\xi'^\dagger \xi''^\dagger) + \lambda^{\xi'} (\xi'^\dagger \xi')^2 + \lambda^{\xi''} (\xi''^\dagger \xi'')^2 \\
& + V(\phi_T, \phi_S) + V(\phi_T, \xi') + V(\phi_T, \xi'') + V(\phi_S, \xi') + V(\phi_S, \xi'') \\
& + V(\phi_T, \phi_S, \xi') + V(\phi_T, \phi_S, \xi'') + V(\phi_T, \xi', \xi'') + V(\phi_S, \xi', \xi''), \tag{B1}
\end{aligned}$$

where $H = \xi', \xi'', \phi_S, \phi_T$, and

$$\begin{aligned}
V(\phi_S, \phi_T) = & \mu_3^2 (\phi_S^\dagger \phi_S)_1 + \mu_4^2 (\phi_T^\dagger \phi_T)_1 + \sum_{x=S,T} \lambda^x [(\phi_x \phi_x^\dagger)^2]_1 + \lambda^{ST} (\phi_S^\dagger \phi_S \phi_T^\dagger \phi_T)_1, \\
V(\phi_T, \xi') = & \lambda^{T\xi'} (\xi'^\dagger \xi') (\phi_T^\dagger \phi_T)_1, \\
V(\phi_T, \xi'') = & \lambda^{T\xi''} (\xi''^\dagger \xi'') (\phi_T^\dagger \phi_T)_1, \\
V(\phi_S, \xi') = & \lambda_2^{S\xi'} \xi'^\dagger \xi' (\phi_S^\dagger \phi_S)_1 + \left\{ \lambda_1^{S\xi'} \xi'^2 (\phi_S^{\dagger 2})_{1'} + \lambda_3^{S\xi'} \xi'^\dagger [(\phi_S^2)_{3s} \phi_S^\dagger]_{1'} + \text{h.c.} \right\}, \\
V(\phi_S, \xi'') = & \lambda_2^{S\xi''} \xi''^\dagger \xi'' (\phi_S^\dagger \phi_S)_1 + \left\{ \lambda_1^{S\xi''} \xi''^2 (\phi_S^{\dagger 2})_{1'} + \lambda_3^{S\xi''} \xi''^\dagger [(\phi_S^2)_{3s} \phi_S^\dagger]_{1''} + \text{h.c.} \right\}, \\
V(\phi_T, \phi_S, \xi') = & \lambda_1^{TS\xi'} \xi'^\dagger [(\phi_S \phi_T)_{3a} \phi_T^\dagger]_{1'} + \lambda_2^{TS\xi'} \xi'^\dagger [(\phi_S \phi_T)_{3s} \phi_T^\dagger]_{1'} + \text{h.c.}, \\
V(\phi_T, \phi_S, \xi'') = & \lambda_1^{TS\xi''} \xi''^\dagger [(\phi_S \phi_T)_{3a} \phi_T^\dagger]_{1'} + \lambda_2^{TS\xi''} \xi''^\dagger [(\phi_S \phi_T)_{3s} \phi_T^\dagger]_{1''} + \text{h.c.}, \\
V(\phi_S, \xi', \xi'') = & \lambda^{S\xi' \xi''} \xi' \xi''^\dagger (\phi_S^\dagger \phi_S)_{1'} + \text{h.c.}, \\
V(\phi_T, \xi', \xi'') = & \lambda^{T\xi' \xi''} \xi' \xi''^\dagger (\phi_T^\dagger \phi_T)_{1'} + \text{h.c.}, \tag{B2}
\end{aligned}$$

where $(\phi_S \phi_S)_{3a} = (0, 0, 0)$.

There are ten neutral Higgs components which will result in ten equations corresponding to the minimal conditions presenting relations between the VEV pattern used in this work

with the Higgs self-couplings. Because of the very large number of the Higgs self-couplings, the VEV pattern assumed in this work is easily guaranteed. Therefore, the lengthy and unnecessary minimal conditions will not be presented here.

In general, the squared mass matrix of the CP-even Higgs bosons are 10×10 matrix, where the main contribution to the SM-like Higgs boson arises from the two Higgs doublets h_u and h_d . Hence, for simplicity in studying the LFV decay of the SM-like Higgs boson, we will choose the regime that these Higgs doublets decouple to other Higgs singlets, namely

$$\lambda^{u\xi'} = \lambda^{d\xi'} = \lambda^{u\xi''} = \lambda^{d\xi''} = \lambda^{Tu} = \lambda^{Td} = \lambda^{Su} = \lambda^{Sd} = 0. \quad (\text{B3})$$

To generate non-zero masses for CP-odd neutral and charged Higgs bosons we adopt a soft term breaking $Z_3 \times Z_{11}$ in the Higgs potential, namely $\mu_{ud}^2 (i\sigma_2 h_u)^T h_d + h.c.$ included in the second line of the Higgs potential (B1). It results in that the masses and eigenstates of all Higgs bosons arising from two Higgs doublet h_u and h_u are the same as those well-known in the 2HDM.

Appendix C: Form factors contributing to the LFV decay rates $e_b \rightarrow e_a \gamma$ ($b > a$), $e_b \rightarrow 3e_a$ and $\mu - e$ conversion in nuclei

The one-loop three-point PV functions [96], called C -functions, which specific definitions were given in Ref. [26]. For cLFV decay processes $e_b \rightarrow e_a \gamma$, where m_a, m_b are the masses of charged leptons $m_{a,b}$ satisfy $m_{a,b}^2/m_W^2 \ll 1$ and $m_{a,b}^2/m_\varphi^2 \ll 1$, the C -functions are

$$\begin{aligned} C_0 &= \frac{t-1-t \ln t}{M_2^2(t-1)^2}, \quad C_1 = C_2 = -\frac{3t^2-4t+1-2t^2 \ln t}{4(t-1)^3 M_2^2}, \\ C_{11} &= C_{22} = 2C_{12} = \frac{11t^3-18t^2+9t-2-6t^3 \ln t}{18M_2^2(t-1)^4}, \end{aligned} \quad (\text{C1})$$

where $t = M_1^2/M_2^2$. The value $t = 1$ gives $C_0 = -1/(2M_2^2)$, $C_1 = 1/(6M_2^2)$, and $C_{11} = -1/(12M_2^2)$.

Contributions from W and φ^\pm bosons to the $\text{Br}(e_b \rightarrow e_a \gamma)$ defined as $D_{(ba)L,R}$ given in Eq. (55) are calculated based on the general form given in Ref. [75], where $C_{(ba)L,R} = \frac{g^2 e m_b}{32\pi^2 m_W^2} \times D_{(ba)L,R}$ and $C_{(ba)L,R}$ is calculated as follows

$$C_{(ba)L}^W = -\frac{eg^2 m_a}{32\pi^2 m_W^2} \sum_{i=1}^9 U_{bi}^{\nu*} U_{ai}^\nu [2(C_{12} + C_{22} - C_1)m_W^2 + m_b^2(C_{11} + C_{12} + C_1)]$$

$$\begin{aligned}
& +m_{n_i}^2(C_0 + C_1 + 2C_2 + C_{12} + C_{22})], \\
C_{(ba)R}^W &= -\frac{eg^2m_b}{32\pi^2m_W^2} \sum_{i=1}^9 U_{bi}^{\nu*} U_{ai}^\nu [2(C_{11} + C_{12} - C_2)m_W^2 + m_a^2(C_{12} + C_{22} + C_2) \\
& +m_{n_i}^2(C_0 + 2C_1 + C_2 + C_{11} + C_{12})] \tag{C2}
\end{aligned}$$

with $C_{0,a,ab} = C_{0,a,ab}(m_{n_i}, m_W, m_W)$, and

$$\begin{aligned}
C_{(ba)L}^\varphi &= -\frac{m_a eg^2}{32\pi^2 m_W^2} \sum_{i=1}^9 U_{bi}^{\nu*} U_{ai}^L \times \{t_\beta^2 m_b^2 (C_1 + C_{11} + C_{12}) \\
& + m_{n_i}^2 [t_\beta^{-2} (C_2 + C_{12} + C_{22}) - (C_0 + C_1 + C_2)]\}, \\
C_{(ba)R}^\varphi &= -\frac{m_b eg^2}{32\pi^2 m_W^2} \sum_{i=1}^9 U_{bi}^{\nu*} U_{ai}^L \times \{t_\beta^2 m_a^2 (C_2 + C_{12} + C_{22}) \\
& + m_{n_i}^2 [t_\beta^{-2} (C_1 + C_{11} + C_{12}) - (C_0 + C_1 + C_2)]\} \tag{C3}
\end{aligned}$$

with $C_{0,a,ab} = C_{0,a,ab}(m_{n_i}, m_\varphi, m_\varphi)$. In the limit $\frac{m_a^2}{m_W^2}, \frac{m_b^2}{m_W^2} = 0$, $C_{(ba)L,R}^W$ is consistent with that given in [97–99]. Also, with $t_{\varphi,i} = \frac{m_{n_i}^2}{m_\varphi^2}$, $C_{(ba)L,R}^\varphi$ have consistent forms with Ref. [99].

Loop functions relating with only gauge bosons are [48, 49]:

$$\begin{aligned}
F_\gamma(x) &= \frac{x(7x^2 - x - 12)}{12(1-x)^3} - \frac{x^2(x^2 - 10x + 12)}{6(1-x)^4} \ln x, \\
G_\gamma(x) &= -\frac{x(2x^2 + 5x - 1)}{4(1-x)^3} - \frac{3x^3}{2(1-x)^4} \ln x, \\
F_Z(x) &= -\frac{5x}{2(1-x)} - \frac{5x^2}{2(1-x)^2} \ln x, \\
G_Z(x, y) &= -\frac{1}{2(x-y)} \left[\frac{x^2(1-y)}{1-x} \ln x - \frac{y^2(1-x)}{1-y} \ln y \right], \\
H_Z(x, y) &= \frac{\sqrt{xy}}{4(x-y)} \left[\frac{x^2 - 4x}{1-x} \ln x - \frac{y^2 - 4y}{1-y} \ln y \right], \\
F_{\text{box}}(x, y) &= \frac{1}{x-y} \left\{ \left(4 + \frac{xy}{4} \right) \left[\frac{1}{1-x} + \frac{x^2}{(1-x)^2} \ln x - \frac{1}{1-y} - \frac{y^2}{(1-y)^2} \ln y \right] \right. \\
& \quad \left. - 2xy \left[\frac{1}{1-x} + \frac{x}{(1-x)^2} \ln x - \frac{1}{1-y} - \frac{y}{(1-y)^2} \ln y \right] \right\}, \\
F_{X\text{box}}(x, y) &= -\frac{1}{x-y} \left\{ \left(1 + \frac{xy}{4} \right) \left[\frac{1}{1-x} + \frac{x^2}{(1-x)^2} \ln x - \frac{1}{1-y} - \frac{y^2}{(1-y)^2} \ln y \right] \right. \\
& \quad \left. - 2xy \left[\frac{1}{1-x} + \frac{x}{(1-x)^2} \ln x - \frac{1}{1-y} - \frac{y}{(1-y)^2} \ln y \right] \right\} \\
G_{\text{box}}(x, y) &= \frac{-\sqrt{xy}}{x-y} \left\{ (4 + xy) \left[\frac{1}{1-x} + \frac{x \ln x}{(1-x)^2} - \frac{1}{1-y} - \frac{y \ln y}{(1-y)^2} \right] \right.
\end{aligned}$$

$$-2 \left[\frac{1}{1-x} + \frac{x^2 \ln x}{(1-x)^2} - \frac{1}{1-y} - \frac{y^2 \ln y}{(1-y)^2} \right] \}. \quad (\text{C4})$$

The loop functions relating with both charged gauge and Higgs bosons are included in Refs. [51, 52]. Here, we use the results given in Ref. [51] and the analytic functions given in Ref. [80] to cast the contributions to the Higgs and gauge bosons into the analytic functions summarized in the following.

For photon, the off-shell form factors are

$$\begin{aligned} F_\gamma^L(x) &= F_\gamma^R(x) = F_\gamma(x), \\ \overline{F}_\gamma^L(x) &= \overline{F}_\gamma^R(x) = -\frac{-11x^3 + 18x^2 - 9x + 2 + 6x^3 \ln(x)}{36(x-1)^4}, \\ (F_\gamma^{ba,X}) &= \sum_{i=1}^9 U_{bi}^{\nu*} U_{ai}^\nu \left[F_\gamma^X(x_{w,i}) + t_\beta^{-2} \overline{F}_\gamma^X(x_{\varphi,i}) \right], \end{aligned} \quad (\text{C5})$$

where $X = L, R$, $x_{w,i} \equiv m_{n_i}^2/m_W^2$, and $x_{\varphi,i} \equiv m_{n_i}^2/m_\varphi^2$.

The on-shell form factors from photon are:

$$\begin{aligned} G_\gamma^L(x) &= G_\gamma^R(x) = G_\gamma(x), \\ \overline{G}_\gamma^L(x) &= \overline{G}_\gamma^R(x) = 2x \left[f_s(x) + t_\beta^{-2} \tilde{f}_s(x) \right], \\ G_\gamma^{ba,X} &= \sum_{i=1}^9 U_{bi}^{\nu*} U_{ai}^\nu \left[G_\gamma^X(x_{w,i}) + \overline{G}_\gamma^X(x_{\varphi,i}) \right]. \end{aligned} \quad (\text{C6})$$

For Z -boson form factors, non-zero contributions are:

$$\begin{aligned} F_Z^L(x) &= F_Z(x), \quad G_Z^L(x) = G_Z(x), \quad H_Z^L(x) = H_Z(x), \\ \overline{G}_Z^L(x) &= -\frac{1}{x-y} \left[\frac{x \ln(x)}{x-1} - \frac{y \ln(y)}{y-1} \right], \\ \overline{G}_Z^R(x) &= \frac{1}{x-y} \left[\frac{x^2 \ln(x)}{x-1} - \frac{y^2 \ln(y)}{y-1} \right], \\ F_Z^{ba,L} &= \sum_{i,j=1}^9 U_{bj}^{\nu*} U_{ai}^\nu \left\{ \delta_{ij} F_Z^L(x_{w,i}) \right. \\ &\quad \left. + D_{ij} \left[G_Z(x_{w,i}, x_{w,j}) + \frac{m_W^2}{2m_\varphi^2 t_\beta^2} \overline{G}_Z(x_{\varphi,i}, x_{\varphi,j}) \right] + D_{ij}^* H_Z(x_{w,i}, x_{w,j}) \right\}, \\ F_Z^{ba,R} &= \sum_{i,j=1}^9 U_{bj}^{\nu*} U_{ai}^\nu \left\{ D_{ij} \left[\frac{m_{e_a} m_{e_b} t_\beta^2}{4m_W^2} \overline{G}_Z^R(x_{\varphi,i}, x_{\varphi,j}) \right] \right\}. \end{aligned} \quad (\text{C7})$$

Leptonic Box Formfactors relating with the four body decays into three leptons:

$$F_{\text{Xbox}}^{LL}(x, y) = F_{\text{Xbox}}(x, y), \quad (\text{C8})$$

$$\begin{aligned} \overline{F}_{\text{Xbox}}^{LL}(x, y, \lambda_\varphi) = & -\frac{2xy}{t_\beta^2} \left[\frac{x(x+4)\ln(x)}{4(x-1)(x-\lambda_\varphi)(x-y)} + \frac{y(y+4)\ln(y)}{4(y-1)(y-\lambda_\varphi)(y-x)} \right. \\ & \left. + \frac{\lambda_\varphi(\lambda_\varphi+4)\ln(\lambda_\varphi)}{4(\lambda_\varphi-1)(\lambda_\varphi-x)(\lambda_\varphi-y)} \right] + \frac{xy}{4\lambda_\varphi(x-y)t_\beta^4} \left[-\frac{x^2\ln(x)}{(x-1)^2} + \frac{y^2\ln(y)}{(y-1)^2} \right], \end{aligned} \quad (\text{C9})$$

$$\begin{aligned} \overline{F}_{\text{Xbox}}^{RL}(x, y, \lambda_\varphi) = & \frac{m_{e_a}m_{e_b}t_\beta^2}{4m_W^2} \left[\frac{x^2(2y+1)\ln(x)}{(x-1)(\lambda_\varphi-x)(x-y)} + \frac{(2x+1)y^2\ln(y)}{(y-1)(\lambda_\varphi-y)(y-x)} \right. \\ & \left. - \frac{\lambda_\varphi(\lambda_\varphi+2xy)\ln(\lambda_\varphi)}{(\lambda_\varphi-1)(\lambda_\varphi-x)(\lambda_\varphi-y)} \right], \end{aligned} \quad (\text{C10})$$

where $\lambda_\varphi \equiv m_\varphi^2/m_W^2$. The total contributions to the $\mu \rightarrow 3e$ decay amplitude are

$$\begin{aligned} F_{\text{box}}^{\mu e e e, LL} = & \sum_{i,j=1}^9 U_{bi}^{\nu*} U_{ai}^\nu U_{aj}^{\nu*} U_{aj}^\nu \left\{ G_{\text{box}}(x_{w,i}, x_{w,j}) - 2 \left[F_{\text{Xbox}}(x_{w,i}, x_{w,j}) + \overline{F}_{\text{Xbox}}^{LL}(x_{\varphi,i}, x_{\varphi,j}, \lambda_\varphi) \right] \right\}, \\ F_{\text{box}}^{\mu e e e, RL} = & \sum_{i,j=1}^9 U_{bi}^{\nu*} U_{ai}^\nu U_{aj}^{\nu*} U_{aj}^\nu \left[-2\overline{F}_{\text{Xbox}}^{RL}(x_{\varphi,i}, x_{\varphi,j}, \lambda_\varphi) \right]. \end{aligned} \quad (\text{C11})$$

In the formula Eq. (56), we ignore all terms containing at least one of the following suppressed factors: m_e^2/m_W^2 , $m_e m_\mu/m_W^2$, m_e/m_μ , for example $F_Z^{ee,R}$, $G_Z^{ee,R}$ and $F_{\text{box}}^{\mu e e e, RL}$.

The semi-leptonic box formfactors relating with one-loop contributions to the $\mu - e$ conversion rate in nuclei are:

$$F_{\text{box}}^{LL}(x, y) = F_{\text{box}}(x, y), \quad (\text{C12})$$

$$\begin{aligned} \overline{F}_{1,\text{box}}^{LL}(x, y, \lambda_\varphi) = & -\frac{xy}{2} \left[\frac{x\ln(x)}{(x-\lambda_\varphi)(x-y)} + \frac{y\ln(y)}{(y-\lambda_\varphi)(y-x)} + \frac{\lambda_\varphi\ln(\lambda_\varphi)}{(\lambda_\varphi-x)(\lambda_\varphi-y)} \right] \\ & + \frac{\lambda_\varphi xy}{4(x-y)t_\beta^4} \left[-\frac{x^2\ln(x)}{(x-1)^2} + \frac{y^2\ln(y)}{(y-1)^2} \right], \end{aligned} \quad (\text{C13})$$

leading to the following total one-loop contributions

$$F_{\text{Box}}^{\mu e u u} = \sum_{i=1}^9 \sum_{d_a=d,s,b} U_{2i}^{\nu*} U_{1i}^\nu V_{ud_a} V_{ud_a}^* \left[F_{\text{box}}(x_{w,i}, x_{d_a}) + \overline{F}_{1,\text{box}}^{LL}(x_{\varphi,i}, x_{d_a}, \lambda_\varphi) \right], \quad (\text{C14})$$

$$F_{\text{Box}}^{\mu e d d} = \sum_{i=1}^9 \sum_{u_a=u,c,t} U_{2i}^{\nu*} U_{1i}^\nu V_{du_a} V_{du_a}^* \left[F_{\text{Xbox}}(x_{w,i}, x_{u_a}) + \overline{F}_{\text{Xbox}}^{LL}(x_{\varphi,i}, x_{u_a}, \lambda_\varphi) \right]. \quad (\text{C15})$$

In the numerical investigation, numerical values of the mixing matrix V and quark masses are collected from Ref. [9], namely we use the central values as follows:

$$V \simeq \begin{pmatrix} 0.974349 & 0.2265 & 0.00132842 - 0.00336345i \\ -0.2265 & 0.974349 & 0.0405288 \\ 0.00785135 + 0.00336345i & -0.0405288 & 1. \end{pmatrix},$$

and $m_{u,c,t} = 2.16 \times 10^{-3}, 1.27, 172.76$ [GeV], and $m_{d,s,b} = 4.67 \times 10^{-3}, 0.093, 4.18$ [GeV].

Appendix D: $\Delta_{L,R}$ for $h \rightarrow \mu\tau$

In this part, we will identify our notation to those defined by LoopTools [100], using the result given in Ref. [83]. For the notations of internal momentum k and external momenta $p_{1,2}$ given in Ref. [83], the PV functions is redefined as follows

$$B_\mu^{(i)} \equiv B_1^{(i)} \times (-1)^i p_{i\mu}, \quad C_\mu \equiv \sum_{i=1}^2 C_i (-1)^i p_{i\mu}, \quad (\text{D1})$$

i.e., the two PV functions $B_1^{(1)}$ and C_1 have opposite signs with those defined in Ref. [83]. All of the PV-functions in this work is just the PV-functions denoted by LoopTools: $B_1^{(i)} = B(p_i^2; M_0^2, M_i^2)$, $C_{0,1,2} = C_{0,1,2}(p_1^2, (p_1 + p_2)^2, p_2^2; M_0^2, M_1^2, M_2^2)$, $B_0 = B_0(p_i^2; M_0^2, M_i^2)$, and $B_0^{(12)} = B_0((p_1 + p_2)^2; M_1^2, M_2^2)$. We will use these functions for the next calculations. Denoting that $\Delta_{L,R}^{(i)} \equiv \Delta_{(ab)L,R}^{(i)}$ for short, the private contributions of all diagrams in Fig. 9 to the LFVH decay amplitude are as follows

$$\begin{aligned} \Delta_L^{(1)} &= \frac{g^3 m_a}{64\pi^2 m_W^3} \times [\sin(\beta - \alpha)] \\ &\times \sum_{i=1}^9 U_{ai}^\nu U_{bi}^{\nu*} \left\{ m_{n_i}^2 \left(B_0^{(1)} + B_0^{(2)} + B_1^{(1)} \right) + m_b^2 B_1^{(2)} - (2m_W^2 + m_h^2) m_{n_i}^2 C_0 \right. \\ &- \left[m_{n_i}^2 (2m_W^2 + m_h^2) + 2m_W^2 (2m_W^2 + m_a^2 - m_b^2) \right] C_1 \\ &\left. - \left[2m_W^2 (m_a^2 - m_h^2) + m_b^2 m_h^2 \right] C_2 \right\}, \end{aligned} \quad (\text{D2})$$

$$\begin{aligned} \Delta_R^{(1)} &= \frac{g^3 m_b}{64\pi^2 m_W^3} \times [\sin(\beta - \alpha)] \\ &\times \sum_{i=1}^9 U_{ai}^\nu U_{bi}^{\nu*} \left\{ m_{n_i}^2 \left(B_0^{(1)} + B_0^{(2)} + B_1^{(2)} \right) + m_a^2 B_1^{(1)} - (2m_W^2 + m_h^2) m_{n_i}^2 C_0 \right. \\ &- \left[2m_W^2 (m_b^2 - m_h^2) + m_a^2 m_h^2 \right] C_1 \\ &\left. - \left[m_{n_i}^2 (2m_W^2 + m_h^2) + 2m_W^2 (2m_W^2 - m_a^2 + m_b^2) \right] C_2 \right\}, \end{aligned} \quad (\text{D3})$$

where $B_{0,1}^{(i)} = B_{0,1}(p_i^2; m_{n_i}^2, m_W^2)$ and $C_{0,1,2} = C_{0,1,2}(p_1^2, m_h^2, p_2^2; m_{n_i}^2, m_W^2, m_W^2)$,

$$\begin{aligned} \Delta_L^{(2)} &= \frac{g^3 m_a}{64\pi^2 m_W^3} \times [\cos(\beta - \alpha)] \\ &\times \sum_{i=1}^9 U_{ai}^\nu U_{bi}^{\nu*} \left\{ t_\beta^{-1} m_{n_i}^2 \left(B_1^{(1)} + B_0^{(1)} \right) + (m_\varphi^2 + m_W^2 - m_h^2) (t_\beta^{-1} m_{n_i}^2 C_0 - t_\beta m_b^2 C_2) \right\} \end{aligned}$$

$$- \left[t_\beta^{-1} m_{n_i}^2 (m_W^2 + m_h^2 - m_\varphi^2) + 2t_\beta m_b^2 m_W^2 \right] C_1 \}, \quad (\text{D4})$$

$$\begin{aligned} \Delta_R^{(2)} &= \frac{g^3 m_b}{64\pi^2 m_W^3} \times [\cos(\beta - \alpha)] \times (-1) \\ &\times \sum_{i=1}^9 U_{ai}^\nu U_{bi}^{\nu*} \left\{ t_\beta \left(m_{n_i}^2 B_0^{(1)} + m_a^2 B_1^{(1)} \right) + m_{n_i}^2 [t_\beta (m_\varphi^2 - m_W^2 - m_h^2) + 2t_\beta^{-1} m_W^2] C_0 \right. \\ &- t_\beta [m_a^2 (m_W^2 + m_h^2 - m_\varphi^2) + 2m_W^2 (m_b^2 - m_h^2)] C_1 \\ &\left. + [t_\beta^{-1} m_{n_i}^2 (m_W^2 + m_h^2 - m_\varphi^2) - 2t_\beta m_W^2 m_b^2] C_2 \right\}, \quad (\text{D5}) \end{aligned}$$

where $B_{0,1}^{(1)} = B_{0,1}(p_1^2; m_{n_i}^2, m_W^2)$ and $C_{0,1,2} = C_{0,1,2}(p_1^2, m_h^2, p_2^2; m_{n_i}^2, m_W^2, m_\varphi^2)$,

$$\begin{aligned} \Delta_L^{(3)} &= \frac{g^3 m_a}{64\pi^2 m_W^3} \times \cos(\beta - \alpha) \times (-1) \\ &\times \sum_{i=1}^9 U_{ai}^\nu U_{bi}^{\nu*} \left\{ t_\beta \left(m_{n_i}^2 B_0^{(2)} + m_b^2 B_1^{(2)} \right) + m_{n_i}^2 [t_\beta (m_\varphi^2 - m_W^2 - m_h^2) + 2t_\beta^{-1} m_W^2] C_0 \right. \\ &+ [t_\beta^{-1} m_{n_i}^2 (m_W^2 + m_h^2 - m_\varphi^2) - 2t_\beta m_W^2 m_a^2] C_1 \\ &\left. - t_\beta [m_b^2 (m_W^2 + m_h^2 - m_\varphi^2) + 2m_W^2 (m_a^2 - m_h^2)] C_2 \right\}, \quad (\text{D6}) \end{aligned}$$

$$\begin{aligned} \Delta_R^{(3)} &= \frac{g^3 m_b}{64\pi^2 m_W^3} \times \cos(\beta - \alpha) \\ &\times \sum_{i=1}^9 U_{ai}^\nu U_{bi}^{\nu*} \left\{ t_\beta^{-1} m_{n_i}^2 \left(B_1^{(2)} + B_0^{(2)} \right) + (m_\varphi^2 + m_W^2 - m_h^2) (t_\beta^{-1} m_{n_i}^2 C_0 - t_\beta m_a^2 C_1) \right. \\ &\left. - [t_\beta^{-1} m_{n_i}^2 (m_W^2 + m_h^2 - m_\varphi^2) + 2t_\beta m_a^2 m_W^2] C_2 \right\}, \quad (\text{D7}) \end{aligned}$$

where $B_{0,1}^{(2)} = B_{0,1}(p_2^2; m_{n_i}^2, m_W^2)$ and $C_{0,1,2} = C_{0,1,2}(p_1^2, m_h^2, p_2^2; m_{n_i}^2, m_\varphi^2, m_W^2)$,

$$\Delta_L^{(4)} = \frac{g^2 m_a}{64\pi^2 m_W^3} \times 2\lambda_{h\varphi\varphi} \sum_{i=1}^9 U_{ai}^\nu U_{bi}^{\nu*} m_W [-m_{n_i}^2 (C_0 - t_\beta^{-2} C_1) + t_\beta^2 m_b^2 C_2], \quad (\text{D8})$$

$$\Delta_R^{(4)} = \frac{g^2 m_b}{64\pi^2 m_W^3} \times 2\lambda_{h\varphi\varphi} \sum_{i=1}^9 U_{ai}^\nu U_{bi}^{\nu*} m_W [-m_{n_i}^2 (C_0 - t_\beta^{-2} C_2) + t_\beta^2 m_a^2 C_1], \quad (\text{D9})$$

where $C_{0,1,2} = C_{0,1,2}(p_1^2, m_h^2, p_2^2; m_{n_i}^2, m_\varphi^2, m_W^2)$, and $\lambda_{h\varphi\varphi} = -2m_W \Gamma/gm$ given in table III.

$$\begin{aligned} \Delta_L^{(5)} &= \frac{g^3 m_a}{64\pi^2 m_W^3} \times \frac{c_\alpha}{s_\beta} \sum_{i,j=1}^9 U_{ai}^\nu U_{bj}^{\nu*} \left\{ D_{ij} \left[-m_{n_j}^2 B_0^{(12)} + m_{n_i}^2 B_1^{(1)} + m_j^2 m_W^2 C_0 \right. \right. \\ &+ \left. \left. \left(2m_W^2 (m_{n_i}^2 + m_{n_j}^2) + 2m_{n_i}^2 m_{n_j}^2 - m_a^2 m_{n_j}^2 - m_b^2 m_{n_i}^2 \right) C_1 \right] \right. \\ &\left. + D_{ij}^* m_{n_i} m_{n_j} \left[-B_0^{(12)} + B_1^{(1)} + m_W^2 C_0 + \left(4m_W^2 + m_{n_i}^2 + m_{n_j}^2 - m_a^2 - m_b^2 \right) C_1 \right] \right\}, \end{aligned}$$

$$\begin{aligned}
\Delta_R^{(5)} = & \frac{g^3 m_b}{64\pi^2 m_W^3} \times \frac{c_\alpha}{s_\beta} \sum_{i,j=1}^9 U_{ai}^\nu U_{bj}^{\nu*} \left\{ D_{ij} \left[-m_{n_i}^2 B_0^{(12)} + m_{n_j}^2 B_1^{(2)} + m_{n_i}^2 m_W^2 C_0 \right. \right. \\
& + \left. \left. \left(2m_W^2 (m_{n_i}^2 + m_{n_j}^2) + 2m_{n_i}^2 m_{n_j}^2 - m_a^2 m_{n_j}^2 - m_b^2 m_{n_i}^2 \right) C_2 \right] \right. \\
& \left. + D_{ij}^* m_{n_i} m_{n_j} \left[-B_0^{(12)} + B_1^{(2)} + m_W^2 C_0 + \left(4m_W^2 + m_{n_i}^2 + m_{n_j}^2 - m_a^2 - m_b^2 \right) C_2 \right] \right\}, \tag{D10}
\end{aligned}$$

where D_{ij} is given in Eq. (54), $B_0^{(12)} = B_0(m_h^2; m_{n_i}^2, m_{n_j}^2)$, $B_1^{(1)} = B_1(p_1^2; m_W^2, m_{n_i}^2)$, $B_1^{(2)} = B_1(p_2^2; m_W^2, m_{n_j}^2)$, and $C_{0,1,2} = C_{0,1,2}(p_1^2, m_h^2, p_2^2; m_W^2, m_{n_i}^2, m_{n_j}^2)$,

$$\begin{aligned}
\Delta_L^{(6)} = & \frac{g^3 m_a}{64\pi^2 m_W^3} \times \frac{c_\alpha}{s_\beta} \sum_{i,j=1}^9 U_{ai}^\nu U_{bj}^{\nu*} \left\{ D_{ij} \left[m_{n_j}^2 B_0^{(12)} + (t_\beta^2 + 1) m_b^2 (m_{n_i}^2 + m_{n_j}^2) C_2 \right. \right. \\
& + \left. \left. \left[(t_\beta^2 + 1) m_b^2 m_{n_i}^2 + m_\varphi^2 m_{n_j}^2 + (t_\beta^{-2} + 1) m_{n_i}^2 m_{n_j}^2 \right] C_0 \right. \right. \\
& + \left. \left. \left(m_b^2 m_{n_i}^2 + m_a^2 m_{n_j}^2 + 2t_\beta^{-2} m_{n_i}^2 m_{n_j}^2 \right) C_1 \right] \right. \\
& + D_{ij}^* m_{n_i} m_{n_j} \left[B_0^{(12)} + 2(t_\beta^2 + 1) m_b^2 C_2 + \left[(t_\beta^2 + 1) m_b^2 + m_\varphi^2 + (1 + t_\beta^{-2}) m_{n_j}^2 \right] C_0 \right. \\
& \left. \left. + \left[m_a^2 + m_b^2 + t_\beta^{-2} (m_{n_i}^2 + m_{n_j}^2) \right] C_1 \right] \right\}, \tag{D11}
\end{aligned}$$

$$\begin{aligned}
\Delta_R^{(6)} = & \frac{g^3 m_b}{64\pi^2 m_W^3} \times \frac{c_\alpha}{s_\beta} \sum_{i,j=1}^9 U_{ai}^\nu U_{bj}^{\nu*} \left\{ D_{ij} \left[m_{n_i}^2 B_0^{(12)} + (t_\beta^2 + 1) m_a^2 (m_{n_i}^2 + m_{n_j}^2) C_1 \right. \right. \\
& + \left. \left. \left[(t_\beta^2 + 1) m_a^2 m_{n_j}^2 + m_\varphi^2 m_{n_i}^2 + (t_\beta^{-2} + 1) m_{n_i}^2 m_{n_j}^2 \right] C_0 \right. \right. \\
& + \left. \left. \left(m_a^2 m_{n_j}^2 + m_b^2 m_{n_i}^2 + 2t_\beta^{-2} m_{n_i}^2 m_{n_j}^2 \right) C_2 \right] \right. \\
& + D_{ij}^* m_{n_i} m_{n_j} \left[B_0^{(12)} + 2(t_\beta^2 + 1) m_a^2 C_1 + \left[(t_\beta^2 + 1) m_a^2 + m_\varphi^2 + (t_\beta^{-2} + 1) m_{n_i}^2 \right] C_0 \right. \\
& \left. \left. + \left(m_a^2 + m_b^2 + t_\beta^{-2} (m_{n_i}^2 + m_{n_j}^2) \right) C_2 \right] \right\}, \tag{D12}
\end{aligned}$$

where $B_0^{(12)} = B_0(m_h^2; m_{n_i}^2, m_{n_j}^2)$, and $C_{0,1,2} = C_{0,1,2}(p_1^2, m_h^2, p_2^2; m_\varphi^2, m_{n_i}^2, m_{n_j}^2)$,

$$\begin{aligned}
\Delta_L^{(7+8)} = & \frac{g^3 m_a}{64\pi^2 m_W^3} \times \frac{s_\alpha}{c_\beta} \times \frac{m_b^2}{m_b^2 - m_a^2} \sum_{i=1}^9 U_{ai}^\nu U_{bi}^{\nu*} \\
& \times \left[\left(2m_W^2 + m_{n_i}^2 \right) \left(B_1^{(2)} - B_1^{(1)} \right) + m_b^2 B_1^{(2)} - m_a^2 B_1^{(1)} + 2m_{n_i}^2 \left(B_0^{(2)} - B_0^{(1)} \right) \right], \\
\Delta_R^{(7+8)} = & \frac{m_a}{m_b} \Delta_L^{(7+8)}, \tag{D13}
\end{aligned}$$

where $\Delta_{L,R}^{(7+8)} \equiv \Delta_{L,R}^{(7)} + \Delta_{L,R}^{(8)}$, and $B_{0,1}^{(i)} \equiv B_{0,1}(p_i^2; m_{n_i}^2, m_W^2)$,

$$\Delta_L^{(9+10)} = \frac{g^3 m_a}{64\pi^2 m_W^3} \times \frac{s_\alpha}{c_\beta} \times \frac{1}{m_b^2 - m_a^2}$$

$$\begin{aligned}
& \times \sum_{i=1}^9 U_{ai}^\nu U_{bi}^{\nu*} \left[m_{n_i}^2 \left(2m_b^2 B_0^{(1)} - (m_a^2 + m_b^2) B_0^{(2)} \right) + (t_\beta^{-2} m_{n_i}^2 + t_\beta^2 m_a^2) m_b^2 \left(B_1^{(2)} - B_1^{(1)} \right) \right], \\
\Delta_R^{(9+10)} &= \frac{g^3 m_b}{64\pi^2 m_W^3} \times \frac{s_\alpha}{c_\beta} \times \frac{1}{m_b^2 - m_a^2} \\
& \times \sum_{i=1}^9 U_{ai}^\nu U_{bi}^{\nu*} \left[m_{n_i}^2 \left((m_a^2 + m_b^2) B_0^{(1)} - 2m_a^2 B_0^{(2)} \right) + (t_\beta^{-2} m_{n_i}^2 + t_\beta^2 m_b^2) m_a^2 \left(B_1^{(2)} - B_1^{(1)} \right) \right],
\end{aligned} \tag{D14}$$

where $\Delta_{L,R}^{(9+10)} \equiv \Delta_{L,R}^{(9)} + \Delta_{L,R}^{(10)}$, and $B_{0,1}^{(i)} \equiv B_{0,1}(p_i^2; m_{n_i}^2, m_\varphi^2)$. The analytic forms of $\Delta_{L,R}^{(i)}$ given here were also cross-checked using the FORM package [101, 102].

Divergent cancellation in total $\Delta_{L,R}$ is proved as follows. Note that divergent part appear only in the B -functions. Using notations of divergent part in [83], $\Delta_\epsilon = (1/\epsilon) - \gamma_E + \ln(4\pi)$, we have $\text{div}[B_0^{(1)}] = \text{div}[B_0^{(2)}] = \text{div}[B_0^{(12)}] = \Delta_\epsilon$, and $\text{div}[B_1^{(1)}] = \text{div}[B_1^{(2)}] = -\Delta_\epsilon/2$. For $\Delta_{L,R}^{(5),(6)}$, divergences relating with D_{ij}^* vanish because they contain one of the factors $\sum_j U_{bj}^\nu m_{n_j} U_{cj}^\nu = M_{bc}^{\nu*} = 0$ and $\sum_i U_{ai}^\nu m_{n_i} U_{ci}^{\nu*} = M_{ac}^\nu = 0$ with all $a, b, c = 1, 2, 3$ [37]. Ignoring the overall factor $\frac{g^2 m_a}{64\pi^2 m_W^3}$ the divergent part of $\Delta_L^{(1)}$ is

$$\text{div} \left[\Delta_L^{(1)} \right] = \sin(\beta - \alpha) \sum_{i=1}^9 U_{ai}^\nu U_{bi}^{\nu*} \Delta_\epsilon \left(\frac{3}{2} m_{n_i}^2 + \frac{1}{2} m_b^2 \right) = \frac{3}{2} \sin(\beta - \alpha) \Delta_\epsilon \sum_{i=1}^9 U_{ai}^\nu U_{bi}^{\nu*} m_{n_i}^2, \tag{D15}$$

where the term containing m_b^2 is canceled because of the Glashow-Iliopoulos-Maiani (GIM) mechanism, $\sum_{i=1}^9 U_{ai}^\nu U_{bi}^{\nu*} = \delta_{ab} = 0$ with $a \neq b$. In the similar calculation, we have

$$\begin{aligned}
\text{div} \left[\Delta_L^{(2)} \right] &= \frac{\Delta_\epsilon}{2} t_\beta^{-1} \cos(\beta - \alpha) \sum_{i=1}^9 U_{ai}^\nu U_{bi}^{\nu*} m_{n_i}^2, \\
\text{div} \left[\Delta_L^{(3)} \right] &= -\Delta_\epsilon t_\beta \cos(\beta - \alpha) \sum_{i=1}^9 U_{ai}^\nu U_{bi}^{\nu*} m_{n_i}^2, \\
\text{div} \left[\Delta_L^{(4)} \right] &= \text{div} \left[\Delta_L^{(7+8)} \right] = 0, \\
\text{div} \left[\Delta_L^{(5)} \right] &= -\frac{3\Delta_\epsilon}{2} \times \frac{c_\alpha}{s_\beta} \sum_{i=1}^9 U_{ai}^\nu U_{bi}^{\nu*} m_{n_i}^2, \\
\text{div} \left[\Delta_L^{(6)} \right] &= \Delta_\epsilon \times \frac{c_\alpha}{s_\beta} \sum_{i=1}^9 U_{ai}^\nu U_{bi}^{\nu*} m_{n_i}^2, \\
\text{div} \left[\Delta_L^{(9+10)} \right] &= \Delta_\epsilon \times \frac{s_\alpha}{c_\beta} \sum_{i=1}^9 U_{ai}^\nu U_{bi}^{\nu*} m_{n_i}^2,
\end{aligned} \tag{D16}$$

where we have used some mediate calculations for shortening the formulas of $\text{div}[\Delta_L^{(5,6)}]$, for example,

$$\begin{aligned} \sum_{i,j=1}^9 U_{ai}^\nu U_{bj}^{\nu*} \left(\sum_{c=1}^3 U_{cj}^\nu U_{ci}^{\nu*} \right) m_{n_j}^2 &= \sum_{j=1}^9 U_{bj}^{\nu*} m_{n_j}^2 \sum_{c=1}^3 U_{cj}^\nu \sum_{i=1}^9 U_{ai}^\nu U_{ci}^{\nu*} = \sum_{j=1}^9 U_{aj}^\nu U_{bj}^{\nu*} m_{n_j}^2, \\ \sum_{i,j=1}^9 U_{ai}^\nu U_{bj}^{\nu*} \left(\sum_{c=1}^3 U_{cj}^{\nu*} U_{ci}^\nu \right) m_{n_i} m_{n_j} &= \sum_{c=1}^3 \sum_{i,j=1}^9 (U_{ai}^\nu m_{n_i} U_{ci}^\nu) (U_{cj}^{\nu*} m_{n_j} U_{bj}^{\nu*}) = 0. \end{aligned}$$

The above results are obtained exactly because of the unitary property of the neutrino mixing matrix U^ν . For $\text{div}[\Delta_L^{(2,3)}]$, we have

$$\begin{aligned} t_\beta^{-1} \cos(\beta - \alpha) &= \frac{(1 - s_\beta^2) c_\alpha + c_\beta s_\beta s_\alpha}{s_\beta} = \frac{c_\alpha}{s_\beta} - \sin(\beta - \alpha), \\ t_\beta \cos(\beta - \alpha) &= \frac{(1 - c_\beta^2) s_\alpha + c_\beta s_\beta c_\alpha}{c_\beta} = \frac{s_\alpha}{c_\beta} + \sin(\beta - \alpha). \end{aligned} \quad (\text{D17})$$

Now it is easy to derive that $\text{div}[\Delta_{L,R}] = 0$ for $a \neq b$. For diagonal case of m_D given by the first line of (7) in this work, every formula in (D16) is automatically equal to zero because $\sum_{i=1}^9 U_{ai}^\nu U_{bi}^{\nu*} m_{n_i}^2 = \left(m_D^\dagger m_D \right)_{ab} = 0$ for $a \neq b$, $a, b = 1, 2, 3$.

-
- [1] P. F. Harrison, D. H. Perkins and W. G. Scott, Phys. Lett. B **530** (2002) 167 [hep-ph/0202074].
 - [2] P. F. Harrison and W. G. Scott, Phys. Lett. B **535**, 163 (2002) [hep-ph/0203209].
 - [3] P. F. Harrison and W. G. Scott, Phys. Lett. B **547** (2002) 219 [hep-ph/0210197].
 - [4] P. F. Harrison and W. G. Scott, Phys. Lett. B **557**, 76 (2003) [hep-ph/0302025].
 - [5] E. Ma and G. Rajasekaran, Phys. Rev. D **64**, 113012 (2001) [hep-ph/0106291].
 - [6] K. S. Babu, E. Ma and J. W. F. Valle, Phys. Lett. B **552** (2003) 207 [hep-ph/0206292].
 - [7] G. Altarelli and F. Feruglio, Nucl. Phys. B **720** (2005) 64 [hep-ph/0504165].
 - [8] G. Altarelli and F. Feruglio, Nucl. Phys. B **741**, 215-235 (2006) [arXiv:hep-ph/0512103 [hep-ph]].
 - [9] P. A. Zyla *et al.* [Particle Data Group], PTEP **2020**, no.8, 083C01 (2020)
 - [10] S. Petcov, Eur. Phys. J. C **78**, no.9, 709 (2018) [arXiv:1711.10806 [hep-ph]].
 - [11] B. Adhikary and A. Ghosal, Phys. Rev. D **78**, 073007 (2008) [arXiv:0803.3582 [hep-ph]].

- [12] J. Barry and W. Rodejohann, Phys. Rev. D **81** (2010) 093002 Erratum: [Phys. Rev. D **81** (2010) 119901] [arXiv:1003.2385 [hep-ph]].
- [13] G. Altarelli, F. Feruglio and L. Merlo, Fortsch. Phys. **61** (2013) 507 [arXiv:1205.5133 [hep-ph]].
- [14] E. Ma, Phys. Rev. D **86** (2012) 117301 [arXiv:1209.3374 [hep-ph]].
- [15] M. C. Chen, J. Huang, J. M. O'Bryan, A. M. Wijangco and F. Yu, JHEP **1302** (2013) 021 [arXiv:1210.6982 [hep-ph]].
- [16] Y. H. Ahn, S. K. Kang and C. S. Kim, Phys. Rev. D **87** (2013) no.11, 113012 [arXiv:1304.0921 [hep-ph]].
- [17] S. Morisi, D. V. Forero, J. C. Romão and J. W. F. Valle, Phys. Rev. D **88** (2013) no.1, 016003 [arXiv:1305.6774 [hep-ph]].
- [18] B. Karmakar and A. Sil, Phys. Rev. D **91** (2015) 013004 [arXiv:1407.5826 [hep-ph]].
- [19] A. E. Cárcamo Hernández and R. Martinez, Nucl. Phys. B **905**, 337-358 (2016) [arXiv:1501.05937 [hep-ph]].
- [20] Pramanick Soumita and Raychaudhuri Amitava, Physical Review D **93**, 033007 (2016) [arXiv:hep-ph/1508.02330 [hep-ph]].
- [21] B. Karmakar and A. Sil, Phys. Rev. D **93** (2016) no.1, 013006 [arXiv:1509.07090 [hep-ph]].
- [22] Mukherjee, Ananya and Das, Mrinal Kumar Nucl. Phys. B 913, 643-663 (2016) [arXiv:hep-ph/1512.02384 [hep-ph]].
- [23] M. Aoki and D. Kaneko, PTEP **2021**, no.2, 023B06 (2021) [arXiv:2009.06025 [hep-ph]].
- [24] G. J. Ding, J. N. Lu and J. W. F. Valle, Phys. Lett. B **815**, 136122 (2021) [arXiv:2009.04750 [hep-ph]].
- [25] B. Karmakar and A. Sil, Phys. Rev. D **96** (2017) no.1, 015007 [arXiv:1610.01909 [hep-ph]].
- [26] T. Phong Nguyen, L. T. Hue, D. T. Si and T. T. Thuc, PTEP **2020**, no.3, 033B04 (2020) [arXiv:1711.05588 [hep-ph]].
- [27] S. K. Kang, Y. Shimizu, K. Takagi, S. Takahashi and M. Tanimoto, PTEP **2018**, no.8, 083B01 (2018) [arXiv:1804.10468 [hep-ph]].
- [28] L. Heinrich, H. Schulz, J. Turner and Y. L. Zhou, JHEP **04**, 144 (2019) [arXiv:1810.05648 [hep-ph]].
- [29] L. M. G. De La Vega, R. Ferro-Hernandez and E. Peinado, Phys. Rev. D **99**, no.5, 055044 (2019) [arXiv:1811.10619 [hep-ph]].

- [30] T. Kobayashi, Y. Shimizu, K. Takagi, M. Tanimoto and T. H. Tatsuishi, JHEP **02**, 097 (2020) [arXiv:1907.09141 [hep-ph]].
- [31] R. Korrapati, J. More, U. Rahaman and S. U. Sankar, Eur. Phys. J. C **81**, no.5, 382 (2021) [arXiv:2009.00865 [hep-ph]].
- [32] S. Mishra, M. K. Behera, R. Mohanta, S. Patra and S. Singirala, Eur. Phys. J. C **80**, no.5, 420 (2020) [arXiv:1907.06429 [hep-ph]].
- [33] E. Arganda, A. M. Curiel, M. J. Herrero and D. Temes, Phys. Rev. D **71** (2005) 035011 [hep-ph/0407302].
- [34] J. A. Casas and A. Ibarra, Nucl. Phys. B **618**, 171-204 (2001) [arXiv:hep-ph/0103065 [hep-ph]].
- [35] A. Pilaftsis, Phys. Lett. B **285** (1992) 68.
- [36] E. Arganda, M. J. Herrero, X. Marcano and C. Weiland, Phys. Rev. D **91** (2015) no.1, 015001 [arXiv:1405.4300 [hep-ph]].
- [37] N. H. Thao, L. T. Hue, H. T. Hung and N. T. Xuan, Nucl. Phys. B **921** (2017) 159 [arXiv:1703.00896 [hep-ph]].
- [38] E. Arganda, M. J. Herrero, X. Marcano, R. Morales and A. Szyrkman, Phys. Rev. D **95**, no.9, 095029 (2017) [arXiv:1612.09290 [hep-ph]].
- [39] V. Khachatryan *et al.* [CMS], Phys. Lett. B **763**, 472-500 (2016) [arXiv:1607.03561 [hep-ex]].
- [40] A. M. Sirunyan *et al.* [CMS], JHEP **06**, 001 (2018) [arXiv:1712.07173 [hep-ex]].
- [41] G. Aad *et al.* [ATLAS], Phys. Lett. B **800**, 135069 (2020) [arXiv:1907.06131 [hep-ex]].
- [42] A. M. Sirunyan *et al.* [CMS], Phys. Rev. D **104**, no.3, 032013 (2021) [arXiv:2105.03007 [hep-ex]].
- [43] Q. Qin, Q. Li, C. D. Lü, F. S. Yu and S. H. Zhou, Eur. Phys. J. C **78**, no.10, 835 (2018) [arXiv:1711.07243 [hep-ph]].
- [44] T. Davidek and L. Fiorini, Front. in Phys. **8**, 149 (2020)
- [45] B. Heinemann and Y. Nir, Usp. Fiz. Nauk **189**, no.9, 985-996 (2019) [arXiv:1905.00382 [hep-ph]].
- [46] U. Bellgardt *et al.* [SINDRUM], Nucl. Phys. B **299**, 1-6 (1988)
- [47] A. Blondel *et al.* Research proposal submitted to the Paul Scherrer Institute Research Committee for Particle Physics at the Ring Cyclotron. 104,[arXiv:1301.6113 [physics.ins-det]].
- [48] R. Alonso, M. Dhen, M. B. Gavela and T. Hambye, JHEP **01**, 118 (2013) [arXiv:1209.2679

- [hep-ph]].
- [49] A. Ilakovac and A. Pilaftsis, Nucl. Phys. B **437**, 491 (1995) [arXiv:hep-ph/9403398 [hep-ph]].
- [50] N. Haba, H. Ishida and Y. Yamaguchi, JHEP **11**, 003 (2016) [arXiv:1608.07447 [hep-ph]].
- [51] A. Ilakovac, A. Pilaftsis and L. Popov, Phys. Rev. D **87**, no.5, 053014 (2013) [arXiv:1212.5939 [hep-ph]].
- [52] A. Abada, M. E. Krauss, W. Porod, F. Staub, A. Vicente and C. Weiland, JHEP **11**, 048 (2014) [arXiv:1408.0138 [hep-ph]].
- [53] G. C. Branco, P. M. Ferreira, L. Lavoura, M. N. Rebelo, M. Sher and J. P. Silva, Phys. Rept. **516**, 1-102 (2012) [arXiv:1106.0034 [hep-ph]].
- [54] N. Chen, T. Han, S. Su, W. Su and Y. Wu, JHEP **03**, 023 (2019) [arXiv:1808.02037 [hep-ph]].
- [55] N. Chen, T. Han, S. Li, S. Su, W. Su and Y. Wu, JHEP **08**, 131 (2020) [arXiv:1912.01431 [hep-ph]].
- [56] F. Kling, S. Su and W. Su, JHEP **06**, 163 (2020) [arXiv:2004.04172 [hep-ph]].
- [57] F. Kling, H. Li, A. Pyarelal, H. Song and S. Su, JHEP **06**, 031 (2019) [arXiv:1812.01633 [hep-ph]].
- [58] D. Azevedo, P. Ferreira, M. M. Mühlleitner, R. Santos and J. Wittbrodt, Phys. Rev. D **99**, no.5, 055013 (2019) [arXiv:1808.00755 [hep-ph]].
- [59] M. C. Gonzalez-Garcia and J. W. F. Valle, Phys. Lett. B **216**, 360-366 (1989)
- [60] P. Minkowski, Phys. Lett. B **67**, 421-428 (1977)
- [61] R. N. Mohapatra and G. Senjanovic, Phys. Rev. Lett. **44**, 912 (1980)
- [62] T. Kitabayashi and M. Yasuè, Phys. Rev. D **93**, no.5, 053012 (2016) [arXiv:1512.00913 [hep-ph]].
- [63] E. W. Otten and C. Weinheimer, Rept. Prog. Phys. **71**, 086201 (2008) [arXiv:0909.2104 [hep-ex]].
- [64] M. J. Dolinski, A. W. P. Poon and W. Rodejohann, Ann. Rev. Nucl. Part. Sci. **69**, 219 (2019) [arXiv:1902.04097 [nucl-ex]].
- [65] M. Lattanzi and M. Gerbino, Front. in Phys. **5**, 70 (2018) [arXiv:1712.07109 [astro-ph.CO]].
- [66] M. Tanabashi *et al.* [Particle Data Group], Phys. Rev. D **98**, no.3, 030001 (2018)
- [67] KATRIN collaboration, *KATRIN design report 2004*, FZKA-7090 (2005).
- [68] D. M. Asner *et al.* [Project 8], Phys. Rev. Lett. **114**, no.16, 162501 (2015) [arXiv:1408.5362 [physics.ins-det]].

- [69] J. F. Gunion and H. E. Haber, Phys. Rev. D **67**, 075019 (2003) [arXiv:hep-ph/0207010 [hep-ph]].
- [70] L. Popov, Doctoral Thesis, 135 [arXiv:1312.1068 [hep-ph]].
- [71] A. Ibarra, E. Molinaro and S. T. Petcov, JHEP **09**, 108 (2010) [arXiv:1007.2378 [hep-ph]].
- [72] H. K. Dreiner, H. E. Haber and S. P. Martin, Phys. Rept. **494** (2010) 1 [arXiv:0812.1594 [hep-ph]].
- [73] J. G. Korner, A. Pilaftsis and K. Schilcher, Phys. Rev. D **47** (1993) 1080 [hep-ph/9301289].
- [74] L. Lavoura, Eur. Phys. J. C **29** (2003) 191 [hep-ph/0302221].
- [75] L. T. Hue, L. D. Ninh, T. T. Thuc and N. T. T. Dat, Eur. Phys. J. C **78** (2018) no.2, 128 [arXiv:1708.09723 [hep-ph]].
- [76] A. Vicente, Front. in Phys. **7** (2019) 174 [arXiv:1908.07759 [hep-ph]].
- [77] F. del Aguila, J. I. Illana and M. D. Jenkins, JHEP **01**, 080 (2009) [arXiv:0811.2891 [hep-ph]].
- [78] F. del Aguila, L. Ametller, J. I. Illana, J. Santiago, P. Talavera and R. Vega-Morales, JHEP **07**, 154 (2019) [arXiv:1901.07058 [hep-ph]].
- [79] G. Hernández-Tomé, J. I. Illana, M. Masip, G. López Castro and P. Roig, Phys. Rev. D **101**, no.7, 075020 (2020) [arXiv:1912.13327 [hep-ph]].
- [80] E. Arganda and M. J. Herrero, Phys. Rev. D **73**, 055003 (2006) [arXiv:hep-ph/0510405 [hep-ph]].
- [81] T. Toma and A. Vicente, JHEP **01**, 160 (2014) [arXiv:1312.2840 [hep-ph]].
- [82] K. S. Sun, S. K. Cui, W. Li and H. B. Zhang, Phys. Rev. D **102**, no.3, 035029 (2020) [arXiv:2004.12266 [hep-ph]].
- [83] L. T. Hue, H. N. Long, T. T. Thuc and T. Phong Nguyen, Nucl. Phys. B **907** (2016) 37 [arXiv:1512.03266 [hep-ph]].
- [84] I. F. Ginzburg and I. P. Ivanov, Phys. Rev. D **72**, 115010 (2005) [arXiv:hep-ph/0508020 [hep-ph]].
- [85] A. Arbey, F. Mahmoudi, O. Stal and T. Stefaniak, Eur. Phys. J. C **78**, no.3, 182 (2018) [arXiv:1706.07414 [hep-ph]].
- [86] J. Song and Y. W. Yoon, Phys. Rev. D **100**, no.5, 055006 (2019) [arXiv:1904.06521 [hep-ph]].
- [87] A. M. Sirunyan *et al.* [CMS Collaboration], JHEP **1811**, 115 (2018) [arXiv:1808.06575 [hep-ex]].
- [88] J. Haller, A. Hoecker, R. Kogler, K. Mönig, T. Peiffer and J. Stelzer, Eur. Phys. J. C **78**, no.

- 8, 675 (2018) [arXiv:1803.01853 [hep-ph]].
- [89] W. S. Hou and G. Kumar, Phys. Rev. D **101**, no.9, 095017 (2020) [arXiv:2003.03827 [hep-ph]].
- [90] A. Crivellin, D. Müller and C. Wiegand, JHEP **06**, 119 (2019) [arXiv:1903.10440 [hep-ph]].
- [91] G. Altarelli and F. Feruglio, Rev. Mod. Phys. **82**, 2701 (2010) [arXiv:1002.0211 [hep-ph]].
- [92] H. Ishimori, T. Kobayashi, H. Ohki, Y. Shimizu, H. Okada and M. Tanimoto, Prog. Theor. Phys. Suppl. **183**, 1 (2010) [arXiv:1003.3552 [hep-th]].
- [93] S. F. King and C. Luhn, JHEP **1109** (2011) 042 [arXiv:1107.5332 [hep-ph]].
- [94] F. Feruglio, C. Hagedorn, Y. Lin and L. Merlo, Nucl. Phys. B **809**, 218 (2009) [arXiv:0807.3160 [hep-ph]].
- [95] F. Feruglio, C. Hagedorn, Y. Lin and L. Merlo, Nucl. Phys. B **832**, 251 (2010) [arXiv:0911.3874 [hep-ph]].
- [96] G. Passarino and M. J. G. Veltman, Nucl. Phys. B **160**, 151 (1979).
- [97] A. Ibarra, E. Molinaro and S. T. Petcov, Phys. Rev. D **84** (2011) 013005 [arXiv:1103.6217 [hep-ph]].
- [98] B. He, T. P. Cheng and L. F. Li, Phys. Lett. B **553** (2003) 277 [hep-ph/0209175].
- [99] A. Crivellin, M. Hoferichter and P. Schmidt-Wellenburg, Phys. Rev. D **98**, no. 11, 113002 (2018) [arXiv:1807.11484 [hep-ph]].
- [100] T. Hahn and M. Perez-Victoria, Comput. Phys. Commun. **118**, 153 (1999) [hep-ph/9807565].
- [101] J. A. M. Vermaseren, “New features of FORM,” math-ph/0010025.
- [102] J. Kuipers, T. Ueda, J. A. M. Vermaseren and J. Vollinga, Comput. Phys. Commun. **184**, 1453 (2013) [arXiv:1203.6543 [cs.SC]].